Available online at www.sciencedirect.com
ScienceDirect
Comput. Methods Appl. Mech. Engrg. 197 (2008) 959–978
Computer methods in applied mechanics and engineering
www.elsevier.com/locate/cma

Edge singularities in 3-D elastic anisotropic and multi-material domains

Netta Omer, Zohar Yosibash *

Pearlstone Center for Aeronautical Engineering Studies, Department of Mechanical Engineering, Ben-Gurion University, Beer-Sheva 84105, Israel

Received 17 April 2007; received in revised form 31 July 2007; accepted 25 September 2007
Available online 1 October 2007

Abstract

The solution to elasticity problems in three-dimensional (3-D) polyhedral multi-material anisotropic domains in the vicinity of an edge is addressed. It includes eigen-functions (similar to 2-D domains) complemented by shadow-functions and their associated edge stress intensity functions (ESIFs), which are functions along the edge. These can be complex and are of major engineering importance in composite materials because failure theories directly or indirectly involve them.

The p-version finite-element methods presented in Yosibash and Omer [Z. Yosibash, N. Omer. Numerical methods for extracting edge stress intensity functions in anisotropic three-dimensional domains. Comput. Methods Appl. Mech. Engrg., 196 (2007) 3624–3649] are extended herein to compute complex eigen-functions and shadows and applied to multi-material anisotropic interfaces. The quasidual function method [M. Costabel, M. Dauge, Z. Yosibash. A quasidual function method for extracting edge stress intensity functions. SIAM J. Math. Anal. 35(5) (2004) 1177–1202] is also extended for extracting complex ESIFs from finite element solutions.

Numerical examples for 3-D isotropic and anisotropic multi-material interfaces are provided for which the complex eigen-pairs and shadow functions are numerically computed and ESIFs extracted. These examples show the efficiency and high accuracy of the numerical approximations.

Keywords: Edge stress intensity functions; p-FEM; Composite materials; Fracture mechanics

1. Introduction

Elastic solutions for realistic three-dimensional (3-D) domains in the vicinity of an edge (as a crack front for example) are of major engineering importance because these are associated with failure initiation and propagation in brittle materials. To the best of our knowledge the number of publications addressing edge singularities in 3-D anisotropic multi-material interfaces is very limited. These works do not address the complete elastic solution and are mainly interested in the first most singular stress intensity pointwise values. The available numerical methods all extract pointwise values of SIFs along the 3-D singular edges, and some employ restrictive assumptions of plane stress/strain situations. Among works applying plane strain/stress assumptions we refer to [6,5,7]. In Ref. [6], the energy release rate is extended to 3-D interface crack between dissimilar anisotropic materials for the computation of $K_{\mathrm{I}}, K_{\mathrm{II}}$, and K_{III}. The volume integral, obtained by extending the 2-D J-integral to 3-D domains, was used in [5] and straight or penny-shaped cracks are addressed in [7] by the "near field" integral – in these works bi-material cracks are considered restricted to only modes I and II loading.

SIF extraction for anisotropic cracked domains is reported in [2,8]. Employing the M-integral good pointwise approximations of SIFs are reported in [2], and in [8] anisotropic penny-shaped cracked configurations are investigated based on both the traditional displacement boundary element method and the displacement discontinuity method. Transversely isotropic bi-material cracked domains are investigated in [13] by the dual boundary element method. The fundamental solution for the bi-material solid occupying an infinite region is incorporated into the

* Corresponding author.
E-mail addresses: nettao@bgu.ac.il (N. Omer), zohary@bgu.ac.il (Z. Yosibash).

0045-7825/$ - see front matter © 2007 Elsevier B.V. All rights reserved.
doi:10.1016/j.cma.2007.09.016

dual boundary integral equations and modes I, II, and III SIFs are computed by the crack opening displacements method.

In the vicinity of an edge the 3-D elastic solution may be represented by a family of eigen-functions (denoted primal and are the well known eigen-functions in 2-D domains) with their associated edge stress intensity functions (ESIFs) which are functions along the edge. At 3-D edges the primal eigen-functions are *complemented by shadow-functions* so the series expansion in the vicinity of an edge is given by (see [4,12] and details in Section 2):

$$\tilde{\boldsymbol{u}} = \sum_{i\geqslant 1}\sum_{j\geqslant 0} \partial_3^j A_i(x_3)\boldsymbol{\Phi}_j^{(\alpha_i)}(r,\theta),$$
$$\boldsymbol{\Phi}_j^{(\alpha_i)}(r,\theta) = r^{\alpha_i+j}\boldsymbol{\varphi}_j^{(\alpha_i)}(\theta), \tag{1}$$

where $\tilde{\boldsymbol{u}}$ is the displacement vector in cylindrical coordinates, $A_i(x_3)$ is the edge stress intensity function (ESIF) associated with the ith eigen-pair, the *primal singular function* $\boldsymbol{\Phi}_0^{(\alpha_i)} = r^{\alpha_i}\boldsymbol{\varphi}_0^{(\alpha_i)}(\theta)$ being the well known two-dimensional eigen-function, whereas $\boldsymbol{\Phi}_j^{(\alpha_i)}$, $j \geqslant 1$ are the *shadow functions* of the primal singular function. In isotropic materials one may compute analytically the primal eigen-functions and their shadows in (1) to be used in conjunction with a newly developed quasi-dual function method (QDFM) [4] for extracting ESIFs from finite element solutions. However, in anisotropic materials and multi-material interfaces difficulties are encountered due to the possible existence of complex eigen-pairs on one hand and intractable analytical derivation on the other hand.

In Ref. [11] a numerical method based on the p-version of the finite element method (p-FEM) was presented for the computation of eigen-pairs and shadow functions for anisotropic domains, used for the extraction of ESIFs. For specific pathological cases (one of which is the cracked configuration being of major importance in fracture mechanics) the numerical methods for computing shadow-functions break down because of conceptual difficulties. These difficulties and the required modifications in the numerical methods for their resolution are addressed herein.

Thereafter the numerical method in [11] is extended to complex eigen-pairs and multi-material interfaces. This case is of particular interest when considering cracks at bi-material interfaces, frequently encountered in laminated composites due to debonding occurring between two anisotropic layers. As a result of the complex eigen-pairs the edge stress intensity functions (ESIFs) are complex also, and the efficient and robust QDFM [4,11] is being extended for extracting complex ESIFs.

We start with a brief description on the series expansion of the elastic solution in the vicinity of a 3-D edge in Section 2. Thereafter the weak formulation for the computation of eigen-pairs and their shadows (complex or real) and the discretization by p-FEMs is addressed in Sections 3 and 4. At this point an explanation on the difficulties in the numerical treatment of the pathological cases is provided in Section 4.3 and a remedy is proposed. A numerical example is provided that illustrates the problems and the remedy. Finally, the quasi-dual function method QDFM is extended to extract complex ESIFs in Section 5. Numerical examples for multi-material interfaces involving anisotropic materials are provided in Section 6 for which the complex eigen-pairs and shadow functions are numerically computed and complex ESIFs extracted. These examples show the efficiency and high accuracy of the numerical approximations.

2. Notations and elastic solution in the vicinity of an edge

Consider a domain Ω in which one straight edge $\mathscr{E}$ of interest is present. For simplicity of presentation let the domain be generated as the product $\Omega = G \times I$, where I is the interval $[-1,1]$, and G is a plane bounded sector of opening $\omega \in (0, 2\pi]$ (the case of a crack, $\omega = 2\pi$, is included), as shown in Fig. 1. Of course G may be composed of several materials and any I can be chosen, and the simplified ones have been chosen for simplicity of presentation.

The variables in G and I are (x_1, x_2) and x_3, respectively, and the coordinates (x_1, x_2, x_3) are denoted by $\boldsymbol{x}$. Let (r,θ) be the cylindrical coordinates centered at the vertex of G so that $G \stackrel{\text{def}}{=} \{(x_1,x_2) \in \mathbb{R}^2 | \theta \in (0,\omega)\}$. The *edge* $\mathscr{E}$ of interest is the set $\{\boldsymbol{x} \in \mathbb{R}^3 | r = 0, x_3 \in I\}$. The two flat planes that intersect at the edge $\mathscr{E}$ are denoted by Γ_1 and Γ_2. For future purposes we also define the cylindrical surface Γ_R as follows:

$$\Gamma_R \stackrel{\text{def}}{=} \{\boldsymbol{x} \in \mathbb{R}^3 | r = R,\ \theta \in (0,\omega), x_3 \in I\}. \tag{2}$$

Remark 1. Methods are restricted to geometries where edges are straight lines and the angle ω is fixed along x_3.

To distinguish between the displacement vector in Cartesian or Cylindrical coordinates, we denote these by $\boldsymbol{u} = \{u_1, u_2, u_3\}^{\mathrm{T}}$ and $\tilde{\boldsymbol{u}} = \{u_r, u_\theta, u_{x_3}\}^{\mathrm{T}}$, respectively and

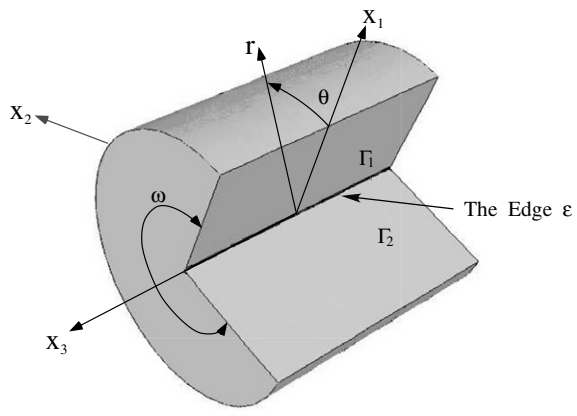

Fig. 1. Domain of interest Ω.

use either of them when convenient. The strains and stresses are denoted by $\boldsymbol{\varepsilon} = \{\varepsilon_{11}, \varepsilon_{22}, \varepsilon_{33}, \gamma_{23}, \gamma_{13}, \gamma_{12}\}^{\mathrm{T}}$, $\tilde{\boldsymbol{\varepsilon}} = \{\varepsilon_{rr}, \varepsilon_{\theta\theta}, \varepsilon_{33}, \gamma_{\theta 3}, \gamma_{r3}, \gamma_{r\theta}\}^{\mathrm{T}}$ and $\boldsymbol{\sigma} = \{\sigma_{11}, \sigma_{22}, \sigma_{33}, \sigma_{23}, \sigma_{13}, \sigma_{12}\}^{\mathrm{T}}$, $\tilde{\boldsymbol{\sigma}} = \{\sigma_{rr}, \sigma_{\theta\theta}, \sigma_{33}, \sigma_{\theta 3}, \sigma_{r3}, \sigma_{r\theta}\}^{\mathrm{T}}$.

Usually, for a general anisotropic domain Hooke's law is given in a Cartesian coordinate system and may be represented also in a cylindrical coordinate system:

$$\boldsymbol{\sigma} = [E]\boldsymbol{\varepsilon}, \quad \text{or } \tilde{\boldsymbol{\sigma}} = [\widetilde{E}]\tilde{\boldsymbol{\varepsilon}}, \tag{3}$$

where $[E]$ (respectively $[\widetilde{E}]$) is a symmetric matrix and $[\widetilde{E}]$ depends on $[E]$ and θ as provided in Appendix A. The Navier–Lamé (N–L) equations for an elastic anisotropic domain without body forces in cylindrical coordinates are [11]:

$$\begin{aligned}
&\Big(-\widetilde{E}_{22}\frac{1}{r} + \widetilde{E}_{15}\partial_3 + \widetilde{E}_{55}r\partial_3^2 + 2\widetilde{E}_{56}\partial_\theta\partial_3 + \widetilde{E}_{66}\frac{1}{r}\partial_\theta^2 \\
&+\widetilde{E}_{11}\partial_r + 2\widetilde{E}_{15}r\partial_r\partial_3 + 2\widetilde{E}_{16}\partial_r\partial_\theta + \widetilde{E}_{11}r\partial_r^2\Big)u_r \\
&+\Big(\widetilde{E}_{26}\frac{1}{r} + (\widetilde{E}_{14} - \widetilde{E}_{24} - \widetilde{E}_{56})\partial_3 + \widetilde{E}_{45}r\partial_3^2 \\
&-(\widetilde{E}_{22} + \widetilde{E}_{66})\frac{1}{r}\partial_\theta + (\widetilde{E}_{25} + \widetilde{E}_{46})\partial_\theta\partial_3 + \widetilde{E}_{26}\frac{1}{r}\partial_\theta^2 - \widetilde{E}_{26}\partial_r \\
&+(\widetilde{E}_{14} + \widetilde{E}_{56})r\partial_r\partial_3 + (\widetilde{E}_{12} + \widetilde{E}_{66})\partial_r\partial_\theta + \widetilde{E}_{16}r\partial_r^2\Big)u_\theta \\
&+\Big((\widetilde{E}_{13} - \widetilde{E}_{23})\partial_3 + \widetilde{E}_{35}r\partial_3^2 - \widetilde{E}_{24}\frac{1}{r}\partial_\theta(\widetilde{E}_{36} + \widetilde{E}_{45})\partial_\theta\partial_3 \\
&+\widetilde{E}_{46}\frac{1}{r}\partial_\theta^2 + (\widetilde{E}_{15} - \widetilde{E}_{25})\partial_r + (\widetilde{E}_{13} + \widetilde{E}_{55})r\partial_r\partial_3 \\
&+(\widetilde{E}_{14} + \widetilde{E}_{56})\partial_r\partial_\theta + \widetilde{E}_{15}r\partial_r^2\Big)u_3 = 0,
\end{aligned} \tag{4}$$

$$\begin{aligned}
&\Big(\widetilde{E}_{26}\frac{1}{r} + (\widetilde{E}_{24} + 2\widetilde{E}_{56})\partial_3 + \widetilde{E}_{45}r\partial_3^2 + (\widetilde{E}_{22} + \widetilde{E}_{66})\frac{1}{r}\partial_\theta \\
&+(\widetilde{E}_{25} + \widetilde{E}_{46})\partial_\theta\partial_3 + \widetilde{E}_{26}\frac{1}{r}\partial_\theta^2 + (2\widetilde{E}_{16} + \widetilde{E}_{26})\partial_r \\
&+(\widetilde{E}_{14} + \widetilde{E}_{56})r\partial_r\partial_3 + (\widetilde{E}_{12} + \widetilde{E}_{66})\partial_r\partial_\theta + \widetilde{E}_{16}r\partial_r^2\Big)u_r \\
&+\Big(-\widetilde{E}_{66}\frac{1}{r} + \widetilde{E}_{46}\partial_3 + \widetilde{E}_{44}r\partial_3^2 + 2\widetilde{E}_{24}\partial_\theta\partial_3 + \widetilde{E}_{22}\frac{1}{r}\partial_\theta^2 \\
&+\widetilde{E}_{66}\partial_r + 2\widetilde{E}_{46}r\partial_r\partial_3 + 2\widetilde{E}_{26}\partial_r\partial_\theta + \widetilde{E}_{66}r\partial_r^2\Big)u_\theta \\
&+\Big(2\widetilde{E}_{36}\partial_3 + \widetilde{E}_{34}r\partial_3^2 + \widetilde{E}_{46}\frac{1}{r}\partial_\theta + (\widetilde{E}_{23} + \widetilde{E}_{44})\partial_\theta\partial_3 \\
&+\widetilde{E}_{24}\frac{1}{r}\partial_\theta^2 + 2\widetilde{E}_{56}\partial_r + (\widetilde{E}_{36} + \widetilde{E}_{45})r\partial_r\partial_3 \\
&+(\widetilde{E}_{25} + \widetilde{E}_{46})\partial_r\partial_\theta + \widetilde{E}_{56}r\partial_r^2\Big)u_3 = 0,
\end{aligned} \tag{5}$$

$$\begin{aligned}
&\Big((\widetilde{E}_{23} + \widetilde{E}_{55})\partial_3 + \widetilde{E}_{35}r\partial_3^2 + \widetilde{E}_{24}\frac{1}{r}\partial_\theta + (\widetilde{E}_{36} + \widetilde{E}_{45})\partial_\theta\partial_3 \\
&+\widetilde{E}_{46}\frac{1}{r}\partial_\theta^2 + (\widetilde{E}_{15} + \widetilde{E}_{25})\partial_r + (\widetilde{E}_{13} + \widetilde{E}_{55})r\partial_r\partial_3 \\
&+(\widetilde{E}_{14} + \widetilde{E}_{56})\partial_r\partial_\theta + \widetilde{E}_{15}r\partial_r^2\Big)u_r + \Big((\widetilde{E}_{45} - \widetilde{E}_{36})\partial_3 \\
&+\widetilde{E}_{34}r\partial_3^2 - \widetilde{E}_{46}\frac{1}{r}\partial_\theta + (\widetilde{E}_{23} + \widetilde{E}_{44})\partial_\theta\partial_3 + \widetilde{E}_{24}\frac{1}{r}\partial_\theta^2 \\
&+(\widetilde{E}_{36} + \widetilde{E}_{45})r\partial_r\partial_3 + (C25 + \widetilde{E}_{46})\partial_r\partial_\theta + \widetilde{E}_{56}r\partial_r^2\Big)u_\theta \\
&+\Big(\widetilde{E}_{35}\partial_3 + \widetilde{E}_{33}r\partial_3^2 + 2\widetilde{E}_{34}\partial_\theta\partial_3 + \widetilde{E}_{44}\frac{1}{r}\partial_\theta^2 + \widetilde{E}_{55}\partial_r \\
&+2\widetilde{E}_{35}r\partial_r\partial_3 + 2\widetilde{E}_{45}\partial_r\partial_\theta + \widetilde{E}_{55}r\partial_r^2\Big)u_3 = 0.
\end{aligned} \tag{6}$$

The N–L equations can be split into three operators as follows:

$$\begin{aligned}
\mathscr{L}(\tilde{\boldsymbol{u}}) = {}& [M_0(\partial_r, \partial_\theta, \theta, \widetilde{E}_{ij})]\tilde{\boldsymbol{u}} + [M_1(\partial_r, \partial_\theta, \theta, \widetilde{E}_{ij})]\partial_3\tilde{\boldsymbol{u}} \\
&+ [M_2(\partial_r, \partial_\theta, \theta, \widetilde{E}_{ij})]\partial_3^2\tilde{\boldsymbol{u}} = 0.
\end{aligned} \tag{7}$$

2.1. Series expansion of the solutions in the vicinity of $\mathscr{E}$

The splitting (7) allows an expression of the solution $\tilde{\boldsymbol{u}}$ as the series (1) in which the *shadow functions* are determined by the following recursive relations (see [4,12]):

$$\begin{aligned}
&[M_0]\boldsymbol{\Phi}_0^{(\alpha_i)} = 0, \\
&[M_0]\boldsymbol{\Phi}_1^{(\alpha_i)} + [M_1]\boldsymbol{\Phi}_0^{(\alpha_i)} = 0, \quad (r,\theta) \in G, \\
&[M_0]\boldsymbol{\Phi}_{j+2}^{(\alpha_i)} + [M_1]\boldsymbol{\Phi}_{j+1}^{(\alpha_i)} + [M_2]\boldsymbol{\Phi}_j^{(\alpha_i)} = 0, \quad j \geqslant 0
\end{aligned} \tag{8}$$

accompanied by homogeneous boundary conditions (BCs) on the two surfaces Γ_1 and Γ_2. The PDE system (8) results in an ODE system for the computation of $\boldsymbol{\varphi}_j^{(\alpha_i)}$ after the substitution of $[M_i]$ and $\boldsymbol{\Phi}_j^{(\alpha_i)}(r,\theta) = r^{\alpha_i+j}\boldsymbol{\varphi}_j^{(\alpha_i)}(\theta)$:

$$\begin{aligned}
&[\mathscr{M}_0]\boldsymbol{\varphi}_0^{(\alpha_i)} = 0, \\
&[\mathscr{M}_0]\boldsymbol{\varphi}_1^{(\alpha_i)} = -[\mathscr{M}_1]\boldsymbol{\varphi}_0^{(\alpha_i)} \quad 0 < \theta < \omega, \\
&[\mathscr{M}_0]\boldsymbol{\varphi}_{j+2}^{(\alpha_i)} = -[\mathscr{M}_1]\boldsymbol{\varphi}_{j+1}^{(\alpha_i)} - [\mathscr{M}_2]\boldsymbol{\varphi}_j^{(\alpha_i)}, \quad j \geqslant 0,
\end{aligned} \tag{9}$$

where

$$\begin{aligned}
[\mathscr{M}_0]\boldsymbol{\varphi}_\gamma^{(\alpha_i)} = {}& ([A_1]\partial_\theta^2 + ((\alpha_i+\gamma)[A_2] + [A_3])\partial_\theta + ((\alpha_i+\gamma)^2[A_4] \\
&+ (\alpha_i+\gamma)[A_5] + [A_6]))\boldsymbol{\varphi}_\gamma^{(\alpha_i)} \\
[\mathscr{M}_1]\boldsymbol{\varphi}_\gamma^{(\alpha_i)} = {}& ([A_7]\partial_\theta + ((\alpha_i+\gamma)[A_8] + [A_9]))\boldsymbol{\varphi}_\gamma^{(\alpha_i)} \\
[\mathscr{M}_2]\boldsymbol{\varphi}_\gamma^{(\alpha_i)} = {}& [A_{10}]\boldsymbol{\varphi}_\gamma^{(\alpha_i)}
\end{aligned} \tag{10}$$

and

$$[A_1] = \begin{pmatrix} \widetilde{E}_{66} & \widetilde{E}_{26} & \widetilde{E}_{46} \\ \widetilde{E}_{26} & \widetilde{E}_{22} & \widetilde{E}_{24} \\ \widetilde{E}_{46} & \widetilde{E}_{24} & \widetilde{E}_{44} \end{pmatrix},$$

$$[A_2] = \begin{pmatrix} 2\widetilde{E}_{16} & \widetilde{E}_{12} + \widetilde{E}_{66} & \widetilde{E}_{14} + \widetilde{E}_{56} \\ \widetilde{E}_{12} + \widetilde{E}_{66} & 2\widetilde{E}_{26} & \widetilde{E}_{25} + \widetilde{E}_{46} \\ \widetilde{E}_{14} + \widetilde{E}_{56} & \widetilde{E}_{25} + \widetilde{E}_{46} & 2\widetilde{E}_{45} \end{pmatrix},$$

$$[A_3] = \begin{pmatrix} 0 & -\widetilde{E}_{22} - \widetilde{E}_{66} & -\widetilde{E}_{24} \\ \widetilde{E}_{22} + \widetilde{E}_{66} & 0 & \widetilde{E}_{46} \\ \widetilde{E}_{24} & -\widetilde{E}_{46} & 0 \end{pmatrix},$$

$$[A_4]=\begin{pmatrix}\widetilde{E}_{11} & \widetilde{E}_{16} & \widetilde{E}_{15}\\ \widetilde{E}_{16} & \widetilde{E}_{66} & \widetilde{E}_{56}\\ \widetilde{E}_{15} & \widetilde{E}_{56} & \widetilde{E}_{55}\end{pmatrix},$$

$$[A_5]=\begin{pmatrix}0 & -\widetilde{E}_{16}-\widetilde{E}_{26} & -\widetilde{E}_{25}\\ \widetilde{E}_{16}+\widetilde{E}_{26} & 0 & \widetilde{E}_{56}\\ \widetilde{E}_{25} & -\widetilde{E}_{56} & 0\end{pmatrix},$$

$$[A_6]=\begin{pmatrix}-\widetilde{E}_{22} & \widetilde{E}_{26} & 0\\ \widetilde{E}_{26} & -\widetilde{E}_{66} & 0\\ 0 & 0 & 0\end{pmatrix},$$

$$[A_7]=\begin{pmatrix}2\widetilde{E}_{56} & (\widetilde{E}_{25}+\widetilde{E}_{46}) & (\widetilde{E}_{36}+\widetilde{E}_{45})\\ (\widetilde{E}_{25}+\widetilde{E}_{46}) & 2\widetilde{E}_{24} & (\widetilde{E}_{23}+\widetilde{E}_{44})\\ (\widetilde{E}_{36}+\widetilde{E}_{45}) & (\widetilde{E}_{23}+\widetilde{E}_{44}) & 2\widetilde{E}_{34}\end{pmatrix},$$

$$[A_8]=\begin{pmatrix}2\widetilde{E}_{15} & (\widetilde{E}_{14}+\widetilde{E}_{56}) & (\widetilde{E}_{13}+\widetilde{E}_{55})\\ (\widetilde{E}_{14}+\widetilde{E}_{56}) & 2\widetilde{E}_{46} & (\widetilde{E}_{36}+\widetilde{E}_{45})\\ (\widetilde{E}_{13}+\widetilde{E}_{55}) & (\widetilde{E}_{36}+\widetilde{E}_{45}) & 2\widetilde{E}_{35}\end{pmatrix}$$

$$[A_9]=\begin{pmatrix}\widetilde{E}_{15} & (\widetilde{E}_{14}-\widetilde{E}_{24}-\widetilde{E}_{56}) & (\widetilde{E}_{13}-\widetilde{E}_{23})\\ (\widetilde{E}_{24}+2\widetilde{E}_{56}) & \widetilde{E}_{46} & 2\widetilde{E}_{36}\\ (\widetilde{E}_{23}+\widetilde{E}_{55}) & -(\widetilde{E}_{36}-\widetilde{E}_{45}) & \widetilde{E}_{35}\end{pmatrix},$$

$$[A_{10}]=\begin{pmatrix}\widetilde{E}_{55} & \widetilde{E}_{45} & \widetilde{E}_{35}\\ \widetilde{E}_{45} & \widetilde{E}_{44} & \widetilde{E}_{34}\\ \widetilde{E}_{35} & \widetilde{E}_{34} & \widetilde{E}_{33}\end{pmatrix}. \tag{11}$$

Notice that $\gamma=0,1,2,\ldots$ correspond to $\boldsymbol{\varphi}_0,\boldsymbol{\varphi}_1,\boldsymbol{\varphi}_2,\ldots$.

For any eigen-value α_i also $-\bar{\alpha}_i$ is an eigen-value with an associated *dual function* which is the solution of $(9)_1$ [4]:

$$\boldsymbol{\Psi}_0^{(\alpha_i)}=c_0^{(\alpha_i)}r^{-\bar{\alpha}_i}\boldsymbol{\psi}_0^{(\alpha_i)}(\theta), \tag{12}$$

where $c_0^{(\alpha_i)}$ is a real coefficient chosen for normalization purposes (will be discussed in the following). The *shadow dual functions* are obtained from $(9)_{2,3}$:

$$\boldsymbol{\Psi}_j^{(\alpha_i)}=r^{-\bar{\alpha}_i+j}\boldsymbol{\psi}_j^{(\alpha_i)}(\theta),\quad j=1,2,\ldots \tag{13}$$

The ODE system (9) is complemented by either homogeneous Dirichlet boundary conditions (clamped-BCs) on Γ_1 and Γ_2, which reads:

$$\boldsymbol{\varphi}_j^{(\alpha_i)}(\theta=0,\omega)=0,\quad j=0,1,\ldots \tag{14}$$

or traction free BCs:

$$\begin{aligned}&[\mathscr{T}_0]\varphi_0=0\\ &[\mathscr{T}_0]\varphi_{j+1}+[\mathscr{T}_1]\varphi_j=0,\quad j\geqslant 0\quad \text{for } \theta=0,\omega,\end{aligned} \tag{15}$$

where

$$\begin{aligned}[\mathscr{T}_0]\boldsymbol{\varphi}_\gamma^{(\alpha_i)}&=([B_1]\partial_\theta+((\alpha_i+\gamma)[B_2]+[B_3]))\boldsymbol{\varphi}_\gamma^{(\alpha_i)},\\ [\mathscr{T}_1]\boldsymbol{\varphi}_\gamma^{(\alpha_i)}&=[B_4]\boldsymbol{\varphi}_\gamma^{(\alpha_i)},\end{aligned} \tag{16}$$

and

$$[B_1]=[A_1],\quad [B_2]=\begin{pmatrix}\widetilde{E}_{16} & \widetilde{E}_{66} & \widetilde{E}_{56}\\ \widetilde{E}_{12} & \widetilde{E}_{26} & \widetilde{E}_{25}\\ \widetilde{E}_{14} & \widetilde{E}_{46} & \widetilde{E}_{45}\end{pmatrix},$$

$$[B_3]=\begin{pmatrix}\widetilde{E}_{26} & -\widetilde{E}_{66} & 0\\ \widetilde{E}_{22} & -\widetilde{E}_{26} & 0\\ \widetilde{E}_{24} & -\widetilde{E}_{46} & 0\end{pmatrix},\quad [B_4]=\begin{pmatrix}\widetilde{E}_{56} & \widetilde{E}_{46} & \widetilde{E}_{36}\\ \widetilde{E}_{25} & \widetilde{E}_{24} & \widetilde{E}_{23}\\ \widetilde{E}_{45} & \widetilde{E}_{44} & \widetilde{E}_{34}\end{pmatrix}. \tag{17}$$

Remark 2. The matrices $[A_i]$ and $[B_i]$ are $\widetilde{E}$ dependent. If material properties are given in a Cartesian coordinate system, $\widetilde{E}$ is represented in terms of $[E]$ and each of the matrices is a combination of 9 independent matrices, multiplying trigonometric functions: $[A_i]+[A_i]_{c1}\cos(\theta)+[A_i]_{c2}\cos(2\theta)+[A_i]_{c3}\cos(3\theta)+[A_i]_{c4}\cos(4\theta)+[A_i]_{s1}\sin(\theta)+[A_i]_{s2}\sin(2\theta)+[A_i]_{s3}\sin(3\theta)+[A_i]_{s4}\sin(4\theta)$. Although in the practical computational scheme we use the decomposition above, herein we condense our notation by using $[\widetilde{E}]$.

3. Computing eigen-pairs

Any eigen-value α and primal eigen-functions $r^{\alpha}\boldsymbol{\varphi}_0^{(\alpha)}$, (and dual eigen-functions $r^{-\alpha}\boldsymbol{\psi}_0^{(\alpha)}$) are the solution of $(9)_1$ with $\gamma=0$, resulting in a quadratic eigen-problem:

$$\begin{aligned}&[A_1]\boldsymbol{\varphi}_0''+(\alpha[A_2]+[A_3])\boldsymbol{\varphi}_0'+(\alpha^2[A_4]+\alpha[A_5]+[A_6])\boldsymbol{\varphi}_0=0,\\ &\theta\in(0,\omega).\end{aligned} \tag{18}$$

The above equation is augmented by either homogeneous Dirichlet BCs, or traction free BCs according to $(15)_1$:

$$\begin{aligned}&\{[B_1]\boldsymbol{\varphi}_0'+(\alpha[B_2]+[B_3])\boldsymbol{\varphi}_0\}_{\theta=0,\omega}=0,\quad \text{Traction free},\\ &\{\boldsymbol{\varphi}_0\}|_{\theta=0,\omega}=0,\quad \text{Homogeneous Dirichlet}.\end{aligned} \tag{19}$$

Since the eigen-pairs may be complex, we formulate the *sesquilinear* form corresponding to (18) on the element level, followed by an assembly procedure. Multiplying (18) by a test function $\bar{\boldsymbol{v}}^{e_i}$ then integrating over the 1-D element (from ω_{i-1} to ω_i) and integrating by parts the second derivative term ($\boldsymbol{\varphi}_0^{e_i}=\boldsymbol{\varphi}_0(\omega_{i-1}\leqslant\theta\leqslant\omega_i)$) one obtains:

$$\begin{aligned}&\left\{\left\{[A_1]\boldsymbol{\varphi}_0^{e_i\prime}\right\}^{\mathrm{T}}\bar{\boldsymbol{v}}^{e_i}\right\}\Big|_{\omega_{i-1}}^{\omega_i}-\int_{\omega_{i-1}}^{\omega_i}\left\{[A_1]\boldsymbol{\varphi}_0^{e_i\prime}\right\}^{\mathrm{T}}\bar{\boldsymbol{v}}^{e_i\prime}\,\mathrm{d}\theta\\ &+\int_{\omega_{i-1}}^{\omega_i}\left\{(\alpha[A_2]+[A_3])\boldsymbol{\varphi}_0^{e_i\prime}\right\}^{\mathrm{T}}\bar{\boldsymbol{v}}^{e_i}\,\mathrm{d}\theta\\ &+\int_{\omega_{i-1}}^{\omega_i}\left\{(\alpha^2[A_4]+\alpha[A_5]+[A_6])\boldsymbol{\varphi}_0^{e_i}\right\}^{\mathrm{T}}\bar{\boldsymbol{v}}^{e_i}\,\mathrm{d}\theta=0.\end{aligned} \tag{20}$$

After enforcing traction free BCs (19):

$$\begin{aligned}\left\{\left\{[A_1]\boldsymbol{\varphi}_0^{e_i\prime}\right\}^{\mathrm{T}}\bar{\boldsymbol{v}}^{e_i}\right\}\Big|_{\omega_{i-1}}^{\omega_i}&=\left\{\left\{[B_1]\boldsymbol{\varphi}_0^{e_i\prime}\right\}^{\mathrm{T}}\bar{\boldsymbol{v}}^{e_i}\right\}\Big|_{\omega_{i-1}}^{\omega_i}\\ &=-\left\{\left\{(\alpha[B_2]+[B_3])\boldsymbol{\varphi}_0^{e_i}\right\}^{\mathrm{T}}\bar{\boldsymbol{v}}^{e_i}\right\}\Big|_{\omega_{i-1}}^{\omega_i},\end{aligned} \tag{21}$$

we define the elemental sesquilinear forms:

$$\begin{aligned}
\mathscr{B}_0^0(\boldsymbol{\varphi}_0^{e_i},\bar{\boldsymbol{v}}^{e_i}) &= -\int_{\omega_{i-1}}^{\omega_i}\left\{[A_1]\boldsymbol{\varphi}_0^{e_i\prime}\right\}^{\mathrm{T}}\bar{\boldsymbol{v}}^{e_i\prime}\,\mathrm{d}\theta+\int_{\omega_{i-1}}^{\omega_i}\left\{[A_3]\boldsymbol{\varphi}_0^{e_i\prime}\right\}^{\mathrm{T}}\bar{\boldsymbol{v}}^{e_i}\,\mathrm{d}\theta\\
&\quad+\int_{\omega_{i-1}}^{\omega_i}\left\{[A_6]\boldsymbol{\varphi}_0^{e_i}\right\}^{\mathrm{T}}\bar{\boldsymbol{v}}^{e_i}\,\mathrm{d}\theta-\left\{\left\{[B_3]\boldsymbol{\varphi}_0^{e_i}\right\}^{\mathrm{T}}\bar{\boldsymbol{v}}^{e_i}\right\}|_{\omega_{i-1}}^{\omega_i},\\
\mathscr{B}_1^0(\boldsymbol{\varphi}_0^{e_i},\bar{\boldsymbol{v}}^{e_i}) &= \int_{\omega_{i-1}}^{\omega_i}\left\{[A_2]\boldsymbol{\varphi}_0^{e_i\prime}\right\}^{\mathrm{T}}\bar{\boldsymbol{v}}^{e_i}\,\mathrm{d}\theta+\int_{\omega_{i-1}}^{\omega_i}\left\{[A_5]\boldsymbol{\varphi}_0^{e_i}\right\}^{\mathrm{T}}\bar{\boldsymbol{v}}^{e_i}\,\mathrm{d}\theta\\
&\quad-\left\{\left\{[B_2]\boldsymbol{\varphi}_0^{e_i}\right\}^{\mathrm{T}}\bar{\boldsymbol{v}}^{e_i}\right\}|_{\omega_{i-1}}^{\omega_i},\\
\mathscr{B}_2^0(\boldsymbol{\varphi}_0^{e_i},\bar{\boldsymbol{v}}^{e_i}) &= \int_{\omega_{i-1}}^{\omega_i}\left\{[A_4]\boldsymbol{\varphi}_0^{e_i}\right\}^{\mathrm{T}}\bar{\boldsymbol{v}}^{e_i}\,\mathrm{d}\theta.
\end{aligned}\tag{22}$$

Finally, assembling all elements, the quadratic sesquilinear eigen-form for the evaluation of the primal and dual eigen-pairs is obtained:

$$\begin{aligned}
&\text{Seek}\quad \alpha\in\mathbb{C},\quad 0\neq\boldsymbol{\varphi}_0\in H^1(0,\omega),\quad \text{s.t.}\quad \forall\boldsymbol{v}\in H^1(0,\omega)\\
&\mathscr{B}_0^0(\boldsymbol{\varphi}_0,\bar{\boldsymbol{v}})+\alpha\mathscr{B}_1^0(\boldsymbol{\varphi}_0,\bar{\boldsymbol{v}})+\alpha^2\mathscr{B}_2^0(\boldsymbol{\varphi}_0,\bar{\boldsymbol{v}})=0
\end{aligned}\tag{23}$$

where H^1 is the Sobolev space, $\mathscr{B}_0^0(\boldsymbol{\varphi}_0,\bar{\boldsymbol{v}})$, $\mathscr{B}_1^0(\boldsymbol{\varphi}_0,\bar{\boldsymbol{v}})$ and $\mathscr{B}_2^0(\boldsymbol{\varphi}_0,\bar{\boldsymbol{v}})$ are the assembled sesquilinear forms resulting from $\mathscr{B}_0^0(\boldsymbol{\varphi}_0^{e_i},\boldsymbol{v}^{e_i})$, $\mathscr{B}_1^0(\boldsymbol{\varphi}_0^{e_i},\boldsymbol{v}^{e_i})$ and $\mathscr{B}_2^0(\boldsymbol{\varphi}_0^{e_i},\boldsymbol{v}^{e_i})$, respectively. In the assembly procedure continuity of the displacement is enforced which insures continuity of traction between two materials in case of multi-material interfaces. The two surfaces $\theta=0,\omega$ are therefore under traction free condition. In the case of Dirichlet BCs the Sobolev space H^1 is replaced by $\overset{\circ}{H}{}^1=\{\boldsymbol{v}|\boldsymbol{v}\in H^1,\boldsymbol{v}(\theta=0,\omega)=\boldsymbol{0}\}$.

3.1. p-FEMs for the solution of the weak eigen-formulation

The eigen-functions are smooth functions, thus the application of p-FEMs for the solution of (23) should result in exponential convergence rates. To this end $\boldsymbol{\varphi}_0=(\,u_0\quad v_0\quad w_0\,)^{\mathrm{T}}$ is expressed in terms of the basis functions $N_k(\xi)$ (integrals of Legendre polynomials) in the standard element:

$$\begin{aligned}
u_0^{e_i}(\xi)&=\sum_{k=1}^{p+1}a_kN_k(\xi),\quad v_0^{e_i}(\xi)=\sum_{k=1}^{p+1}a_{p+1+k}N_k(\xi),\\
w_0^{e_i}(\xi)&=\sum_{k=1}^{p+1}a_{2p+2+k}N_k(\xi)
\end{aligned}\tag{24}$$

or

$$\begin{aligned}
\boldsymbol{\varphi}_0^{e_i}&=\begin{pmatrix}N_1(\xi)\cdots N_{p+1}(\xi) & 0\cdots0 & 0\cdots0\\ 0\cdots0 & N_1(\xi)\cdots N_{p+1}(\xi) & 0\cdots0\\ 0\cdots0 & 0\cdots0 & N_1(\xi)\cdots N_{p+1}(\xi)\end{pmatrix}\\
&\quad\times\begin{pmatrix}a_1\\ \vdots\\ a_{3(p+1)}\end{pmatrix}\overset{\text{def}}{=}[N]\boldsymbol{a}_0^{e_i}.
\end{aligned}\tag{25}$$

Similarly $\bar{\boldsymbol{v}}^{e_i}\overset{\text{def}}{=}[N]\boldsymbol{b}_0^{e_i}$, and $\mathrm{d}\theta=\frac{\omega}{2}\,\mathrm{d}\xi$. Substituting (25) in (23) one obtains the FE formulation of the weak eigen-form:

$$\boldsymbol{a}_0^{\mathrm{T}}(\alpha^2[K_2^0]+\alpha[K_1^0]+[K_0^0])=\boldsymbol{0},\tag{26}$$

where $[K_0^0],[K_1^0],[K_2^0]$ are the assembled matrices corresponding to $[K_0^0]^{e_i},[K_1^0]^{e_i},[K_2^0]^{e_i}$, respectively and $\omega^{e_i}=\omega_i-\omega_{i-1}$.

$$\begin{aligned}
[K_2^0]^{e_i}&=\frac{\omega^{e_i}}{2}\int_{-1}^{1}[N]^{\mathrm{T}}[A_4]^{\mathrm{T}}[N]\mathrm{d}\xi,\\
[K_1^0]^{e_i}&=-\left\{[N]^{\mathrm{T}}[B_2]^{\mathrm{T}}[N]\right\}|_{\omega_{i-1}}^{\omega_i}+\int_{-1}^{1}[N']^{\mathrm{T}}[A_2]^{\mathrm{T}}[N]\mathrm{d}\xi\\
&\quad+\frac{\omega^{e_i}}{2}\int_{-1}^{1}[N]^{\mathrm{T}}[A_5]^{\mathrm{T}}[N]\,\mathrm{d}\xi,\\
[K_0^0]^{e_i}&=-\left\{[N]^{\mathrm{T}}[B_3]^{\mathrm{T}}[N]\right\}|_{\omega_{i-1}}^{\omega_i}-\frac{2}{\omega^{e_i}}\int_{-1}^{1}[N']^{\mathrm{T}}[A_1]^{\mathrm{T}}[N']\mathrm{d}\xi\\
&\quad+\int_{-1}^{1}[N']^{\mathrm{T}}[A_3]^{\mathrm{T}}[N]\mathrm{d}\xi\\
&\quad+\frac{\omega^{e_i}}{2}\int_{-1}^{1}[N]^{\mathrm{T}}[A_6]^{\mathrm{T}}[N]\mathrm{d}\xi.
\end{aligned}\tag{27}$$

$\boldsymbol{a}_0$ is the vector of assembled coefficients of $\boldsymbol{a}_0^{e_i}$. For clamped BCs $[B_2]|_0=[B_2]|_\omega=[B_3]|_0=[B_3]|_\omega=[0]$. The quadratic eigen-problem (26) is solved by a linearization process according to [1]. Setting $\boldsymbol{d}_0=\alpha\boldsymbol{a}_0$ the $(3pQ+3)\times(3pQ+3)$ (Q is the number of elements) quadratic eigen-problem is transformed into a linear $(6pQ+6)\times(6pQ+6)$ "standard eigen-problem":

$$\begin{pmatrix}\boldsymbol{a}_0\\ \boldsymbol{d}_0\end{pmatrix}^{\mathrm{T}}\begin{pmatrix}0 & [K_0^0]\\ I & [K_1^0]\end{pmatrix}=\alpha\begin{pmatrix}\boldsymbol{a}_0\\ \boldsymbol{d}_0\end{pmatrix}^{\mathrm{T}}\begin{pmatrix}I & 0\\ 0 & -[K_2^0]\end{pmatrix}.\tag{28}$$

Because the eigen-pairs may be complex, the complex α and $\boldsymbol{a}_0$ are denoted by: $\alpha=\alpha_{\Re}+\mathrm{i}\alpha_{\Im}$ and $\boldsymbol{a}_0=\boldsymbol{a}_{0_{\Re}}+\mathrm{i}\boldsymbol{a}_{0_{\Im}}$.

3.2. The normalization factor c_0

The dual eigen-functions $\boldsymbol{\psi}_0$ are the solutions of (28) associated with negative eigen-values. The normalization factor $c_0^{(\alpha)}$ is determined so that the primal and dual eigen-functions satisfy an orthonormal condition (see [4,12]) under the integration along a circular curve with the edge being its center:

$$\int_0^{\omega}\left\{\boldsymbol{T}^{\Gamma_R}\boldsymbol{\Phi}_0^{(\alpha)}\cdot\overline{\boldsymbol{\Psi}}_0^{(\alpha)}-\boldsymbol{\Phi}_0^{(\alpha)}\cdot\boldsymbol{T}^{\Gamma_R}\overline{\boldsymbol{\Psi}}_0^{(\alpha)}\right\}R\,\mathrm{d}\theta=1,\tag{29}$$

where $\boldsymbol{T}^{\Gamma_R}$ is Neumann trace operator (related to $\mathscr{L}$) on a circular surface around the edge:

$$\boldsymbol{T}^{\Gamma_R}\tilde{\boldsymbol{u}} \stackrel{\text{def}}{=} \begin{pmatrix}\sigma_{rr}\\ \sigma_{r\theta}\\ \sigma_{r3}\end{pmatrix} = \begin{pmatrix} \frac{1}{r}\widetilde{E}_{12}+\widetilde{E}_{15}\partial_3+\frac{1}{r}\widetilde{E}_{16}\partial_\theta+\widetilde{E}_{11}\partial_r-\frac{1}{r}\widetilde{E}_{16}+\widetilde{E}_{14}\partial_3+\frac{1}{r}\widetilde{E}_{12}\partial_\theta+\widetilde{E}_{16}\partial_r\widetilde{E}_{13}\partial_3+\frac{1}{r}\widetilde{E}_{14}\partial_\theta+\widetilde{E}_{15}\partial_r \\ \frac{1}{r}\widetilde{E}_{26}+\widetilde{E}_{56}\partial_3+\frac{1}{r}\widetilde{E}_{66}\partial_\theta+\widetilde{E}_{16}\partial_r-\frac{1}{r}\widetilde{E}_{66}+\widetilde{E}_{46}\partial_3+\frac{1}{r}\widetilde{E}_{26}\partial_\theta+\widetilde{E}_{66}\partial_r\widetilde{E}_{36}\partial_3+\frac{1}{r}\widetilde{E}_{46}\partial_\theta+\widetilde{E}_{56}\partial_r \\ \frac{1}{r}\widetilde{E}_{25}+\widetilde{E}_{55}\partial_3+\frac{1}{r}\widetilde{E}_{56}\partial_\theta+\widetilde{E}_{15}\partial_r-\frac{1}{r}\widetilde{E}_{56}+\widetilde{E}_{45}\partial_3+\frac{1}{r}\widetilde{E}_{25}\partial_\theta+\widetilde{E}_{56}\partial_r\widetilde{E}_{35}\partial_3+\frac{1}{r}\widetilde{E}_{45}\partial_\theta+\widetilde{E}_{55}\partial_r \end{pmatrix}\begin{pmatrix}u_r\\ u_\theta\\ u_3\end{pmatrix}. \tag{30}$$

The operator $\boldsymbol{T}^{\Gamma_R}$ is split according to $\boldsymbol{T}^{\Gamma_R}=\boldsymbol{T}_0^{\Gamma_R}(\partial_r,\partial_\theta)+\boldsymbol{T}_1^{\Gamma_R}(\partial_r,\partial_\theta)\partial_3$ with:

$$\begin{aligned}\boldsymbol{T}_0^{\Gamma_R}(\partial_r,\partial_\theta)\boldsymbol{\Phi}_j &= \left([T_a]\frac{1}{r}\partial_\theta+[T_b]\partial_r+([T_c]+j[T_b])\frac{1}{r}\right)\boldsymbol{\Phi}_j,\\ \boldsymbol{T}_1^{\Gamma_R}(\partial_r,\partial_\theta)\boldsymbol{\Phi}_j &= [T_d]\boldsymbol{\Phi}_j,\end{aligned} \tag{31}$$

$$\begin{aligned}[T_a]&=\begin{pmatrix}\widetilde{E}_{16}&\widetilde{E}_{12}&\widetilde{E}_{14}\\ \widetilde{E}_{66}&\widetilde{E}_{26}&\widetilde{E}_{46}\\ \widetilde{E}_{56}&\widetilde{E}_{25}&\widetilde{E}_{45}\end{pmatrix}, \quad [T_b]=\begin{pmatrix}\widetilde{E}_{11}&\widetilde{E}_{16}&\widetilde{E}_{15}\\ \widetilde{E}_{16}&\widetilde{E}_{66}&\widetilde{E}_{56}\\ \widetilde{E}_{15}&\widetilde{E}_{56}&\widetilde{E}_{55}\end{pmatrix},\\ [T_c]&=\begin{pmatrix}\widetilde{E}_{12}&-\widetilde{E}_{16}&0\\ \widetilde{E}_{26}&-\widetilde{E}_{66}&0\\ \widetilde{E}_{25}&-\widetilde{E}_{56}&0\end{pmatrix}, \quad [T_d]=\begin{pmatrix}\widetilde{E}_{15}&\widetilde{E}_{14}&\widetilde{E}_{13}\\ \widetilde{E}_{56}&\widetilde{E}_{46}&\widetilde{E}_{36}\\ \widetilde{E}_{55}&\widetilde{E}_{45}&\widetilde{E}_{35}\end{pmatrix}.\end{aligned} \tag{32}$$

Because the eigen-pairs and their duals are independent of x_3 one obtains:

$$\begin{aligned}\boldsymbol{T}^{\Gamma_R}\boldsymbol{\Phi}_0^{(\alpha)} &= \boldsymbol{T}_0^{\Gamma_R}\boldsymbol{\Phi}_0^{(\alpha)} = R^{\alpha-1}\left\{[T_a]\boldsymbol{\varphi}_0'+\alpha[T_b]\boldsymbol{\varphi}_0+[T_c]\boldsymbol{\varphi}_0\right\},\\ \boldsymbol{T}^{\Gamma_R}\overline{\boldsymbol{\Psi}}_0^{(\alpha)} &= \boldsymbol{T}_0^{\Gamma_R}\overline{\boldsymbol{\Psi}}_0^{(\alpha)} = R^{-\alpha-1}\left\{[T_a]\bar{\boldsymbol{\psi}}_0'-\alpha[T_b]\bar{\boldsymbol{\psi}}_0+[T_c]\bar{\boldsymbol{\psi}}_0\right\}.\end{aligned} \tag{33}$$

Inserting (12) and (33) in (29), the expression for the normalization factor c_0 is obtained:

$$\begin{aligned}c_0^{(\alpha)}\Bigg(\int_0^{\omega}&\left\{([T_a]\boldsymbol{\varphi}_0'+\alpha[T_b]\boldsymbol{\varphi}_0+[T_c]\boldsymbol{\varphi}_0)\cdot\bar{\boldsymbol{\psi}}-\boldsymbol{\varphi}_0\right.\\ &\left.\cdot([T_a]\bar{\boldsymbol{\psi}}_0'-\alpha[T_b]\bar{\boldsymbol{\psi}}_0+[T_c]\bar{\boldsymbol{\psi}})\right\}\mathrm{d}\theta\Bigg)=1.\end{aligned} \tag{34}$$

Substituting $c_0=c_{0_\Re}+\mathrm{i}c_{0_\Im}$, $\alpha=\alpha_\Re+\mathrm{i}\alpha_\Im$, $\boldsymbol{\varphi}_0=\boldsymbol{\varphi}_{0_\Re}+\mathrm{i}\boldsymbol{\varphi}_{0_\Im}$ and $\bar{\boldsymbol{\psi}}_0=\boldsymbol{\psi}_{0_\Re}-\mathrm{i}\boldsymbol{\psi}_{0_\Im}$ into (34) the following system is obtained:

$$\begin{cases}c_{0_\Re}^{(\alpha)}I_{c_0}^{\Re}-c_{0_\Im}^{(\alpha)}I_{c_0}^{\Im}=1\\ c_{0_\Re}^{(\alpha)}I_{c_0}^{\Im}+c_{0_\Im}^{(\alpha)}I_{c_0}^{\Re}=0\end{cases}\Rightarrow\begin{cases}c_{0_\Re}^{(\alpha)}=\frac{I_{c_0}^{\Re}}{I_{c_0}^{\Re^2}+I_{c_0}^{\Im^2}}\\ c_{0_\Im}^{(\alpha)}=\frac{-I_{c_0}^{\Im}}{I_{c_0}^{\Re^2}+I_{c_0}^{\Im^2}}\end{cases}, \tag{35}$$

where

$$\begin{aligned}I_{c_0}^{\Re}=&\int_0^{\omega}([T_a]\boldsymbol{\varphi}_{0_\Re}'+\alpha_\Re[T_b]\boldsymbol{\varphi}_{0_\Re}-\alpha_\Im[T_b]\boldsymbol{\varphi}_{0_\Im}+[T_c]\boldsymbol{\varphi}_{0_\Re})\cdot\boldsymbol{\psi}_{0_\Re}\,\mathrm{d}\theta\\ &+\int_0^{\omega}([T_a]\boldsymbol{\varphi}_{0_\Im}'+\alpha_\Re[T_b]\boldsymbol{\varphi}_{0_\Im}+\alpha_\Im[T_b]\boldsymbol{\varphi}_{0_\Re}+[T_c]\boldsymbol{\varphi}_{0_\Im})\cdot\boldsymbol{\psi}_{0_\Im}\,\mathrm{d}\theta\\ &+\int_0^{\omega}\boldsymbol{\varphi}_{0_\Re}\cdot([T_a]\boldsymbol{\psi}_{0_\Re}'-\alpha_\Re[T_b]\boldsymbol{\psi}_{0_\Re}+\alpha_\Im[T_b]\boldsymbol{\psi}_{0_\Im}+[T_c]\boldsymbol{\psi}_{0_\Re})\,\mathrm{d}\theta\\ &+\int_0^{\omega}\boldsymbol{\varphi}_{0_\Im}\cdot([T_a]\boldsymbol{\psi}_{0_\Im}'-\alpha_\Re[T_b]\boldsymbol{\psi}_{0_\Im}-\alpha_\Im[T_b]\boldsymbol{\psi}_{0_\Re}+[T_c]\boldsymbol{\psi}_{0_\Im})\,\mathrm{d}\theta,\end{aligned}$$

$$\begin{aligned}I_{c_0}^{\Im}=&-\int_0^{\omega}([T_a]\boldsymbol{\varphi}_{0_\Re}'+\alpha_\Re[T_b]\boldsymbol{\varphi}_{0_\Re}-\alpha_\Im[T_b]\boldsymbol{\varphi}_{0_\Im}+[T_c]\boldsymbol{\varphi}_{0_\Re})\cdot\boldsymbol{\psi}_{0_\Im}\,\mathrm{d}\theta\\ &+\int_0^{\omega}([T_a]\boldsymbol{\varphi}_{0_\Im}'+\alpha_\Re[T_b]\boldsymbol{\varphi}_{0_\Im}+\alpha_\Im[T_b]\boldsymbol{\varphi}_{0_\Re}+[T_c]\boldsymbol{\varphi}_{0_\Im})\cdot\boldsymbol{\psi}_{0_\Re}\,\mathrm{d}\theta\\ &+\int_0^{\omega}\boldsymbol{\varphi}_{0_\Im}\cdot([T_a]\boldsymbol{\psi}_{0_\Re}'-\alpha_\Re[T_b]\boldsymbol{\psi}_{0_\Re}+\alpha_\Im[T_b]\boldsymbol{\psi}_{0_\Im}+[T_c]\boldsymbol{\psi}_{0_\Re})\,\mathrm{d}\theta\\ &-\int_0^{\omega}\boldsymbol{\varphi}_{0_\Re}\cdot([T_a]\boldsymbol{\psi}_{0_\Im}'-\alpha_\Re[T_b]\boldsymbol{\psi}_{0_\Im}-\alpha_\Im[T_b]\boldsymbol{\psi}_{0_\Re}+[T_c]\boldsymbol{\psi}_{0_\Im})\,\mathrm{d}\theta.\end{aligned} \tag{36}$$

4. Computing complex primal and dual shadow functions

4.1. The weak form for the computation of primal and dual shadow functions

The primal and dual shadow functions $\boldsymbol{\varphi}_\gamma$ and $\boldsymbol{\psi}_\gamma$ are the solutions of system (9) $\boldsymbol{\varphi}_1,\boldsymbol{\psi}_1$ are the solutions of $(9)_2$ whereas $\boldsymbol{\varphi}_\gamma,\boldsymbol{\psi}_\gamma,\gamma\geqslant 2$ are the solutions of $(9)_3$. $\boldsymbol{\psi}_\gamma$ is computed by replacing $(\boldsymbol{\varphi}_{\gamma_\Re}^{(\alpha)}+\mathrm{i}\boldsymbol{\varphi}_{\gamma_\Im}^{(\alpha)})$ and $(\alpha_\Re+\mathrm{i}\alpha_\Im)$ by $(\boldsymbol{\psi}_{\gamma_\Re}^{(\alpha)}+\mathrm{i}\boldsymbol{\psi}_{\gamma_\Im}^{(\alpha)})$ and $(-\alpha_\Re+\mathrm{i}\alpha_\Im)$ in the relevant equation of system (9). Notice that $\alpha_\Re+\mathrm{i}\alpha_\Im$ is known, obtained by solving the eigen-value problem in the previous section. The weak formulation for $\boldsymbol{\varphi}_\gamma^{e_i}$, on the element level, is obtained by multiplying the appropriate equation in (9) by a test function $\bar{\boldsymbol{v}}^{e_i}$ and integrated over ω^{e_i}. Applying integration by parts on the second derivative term one obtains:

$$\begin{aligned}&\left\{([A_1]\boldsymbol{\varphi}_\gamma^{e_i\prime})^{\mathrm{T}}\bar{\boldsymbol{v}}^{e_i}\right\}|_{\omega_{i-1}}^{\omega_i}-\int_{\omega_{i-1}}^{\omega_i}([A_1]\boldsymbol{\varphi}_\gamma^{e_i\prime})^{\mathrm{T}}\bar{\boldsymbol{v}}^{e_i\prime}\,\mathrm{d}\theta\\ &+\int_{\omega_{i-1}}^{\omega_i}[((\alpha+\gamma)[A_2]+[A_3])\boldsymbol{\varphi}_\gamma^{e_i\prime}]^{\mathrm{T}}\bar{\boldsymbol{v}}^{e_i}\,\mathrm{d}\theta\\ &+\int_{\omega_{i-1}}^{\omega_i}[((\alpha+\gamma)^2[A_4]+(\alpha+\gamma)[A_5]+[A_6])\boldsymbol{\varphi}_\gamma^{e_i}]^{\mathrm{T}}\bar{\boldsymbol{v}}^{e_i}\,\mathrm{d}\theta\\ &+\int_{\omega_{i-1}}^{\omega_i}([A_7]\boldsymbol{\varphi}_{\gamma-1}^{e_i\prime})^{\mathrm{T}}\bar{\boldsymbol{v}}^{e_i}\,\mathrm{d}\theta+\int_{\omega_{i-1}}^{\omega_i}[((\alpha+\gamma-1)[A_8]\\ &+[A_9])\boldsymbol{\varphi}_{\gamma-1}^{e_i}]^{\mathrm{T}}\bar{\boldsymbol{v}}^{e_i}\,\mathrm{d}\theta\\ &+\varrho\int_{\omega_{i-1}}^{\omega_i}[([A_{10}])\boldsymbol{\varphi}_{\gamma-2}^{e_i}]^{\mathrm{T}}\bar{\boldsymbol{v}}^{e_i}\,\mathrm{d}\theta=0,\end{aligned} \tag{37}$$

where

$$\varrho=\begin{cases}0 & \gamma=1,\\ 1 & \gamma\geqslant 2.\end{cases} \tag{38}$$

Traction free boundary conditions are applied on each element and by using (16) we represent the first term in (37):

$$\left\{([A_1]\boldsymbol{\varphi}_\gamma^{e_i'})^{\mathrm{T}}\bar{\boldsymbol{v}}^{e_i}\right\}|_{\omega_{i-1}}^{\omega_i} = \left\{([B_1]\boldsymbol{\varphi}_\gamma^{e_i'})^{\mathrm{T}}\bar{\boldsymbol{v}}^{e_i}\right\}|_{\omega_{i-1}}^{\omega_i} = -\left\{[((\alpha+\gamma)[B_2]+[B_3])\boldsymbol{\varphi}_\gamma^{e_i}]^{\mathrm{T}}\bar{\boldsymbol{v}}^{e_i}\right\}|_{\omega_{i-1}}^{\omega_i} - \left\{([B_4]\boldsymbol{\varphi}_{\gamma-1}^{e_i})^{\mathrm{T}}\bar{\boldsymbol{v}}^{e_i}\right\}|_{\omega_{i-1}}^{\omega_i}. \tag{39}$$

The sesquilinear form for the computation of the shadow function $\boldsymbol{\varphi}_\gamma$ is:

$$\text{Seek}\quad \boldsymbol{\varphi}_\gamma \in H^1(0,\omega),\quad \text{s.t.}\quad \mathscr{B}^\gamma(\boldsymbol{\varphi}_\gamma,\bar{\boldsymbol{v}}) = \mathscr{F}^\gamma(\bar{\boldsymbol{v}}),\quad \forall \bar{\boldsymbol{v}} \in H^1(0,\omega) \tag{40}$$

where $\mathscr{B}^\gamma(\boldsymbol{\varphi}_\gamma,\bar{\boldsymbol{v}})$ and $\mathscr{F}^\gamma(\bar{\boldsymbol{v}})$ are the assembled forms of $\mathscr{B}^\gamma(\boldsymbol{\varphi}_\gamma^{e_i},\bar{\boldsymbol{v}}^{e_i})$ and $\mathscr{F}^\gamma(\bar{\boldsymbol{v}}^{e_i})$:

$$\begin{aligned}\mathscr{B}^\gamma(\boldsymbol{\varphi}_\gamma^{e_i},\bar{\boldsymbol{v}}^{e_i}) = &-\int_{\omega_{i-1}}^{\omega_i}([A_1]\boldsymbol{\varphi}_\gamma^{e_i'})^{\mathrm{T}}\bar{\boldsymbol{v}}^{e_i\prime}\,\mathrm{d}\theta + \int_{\omega_{i-1}}^{\omega_i}[((\alpha+\gamma)[A_2]\\ &+[A_3])\boldsymbol{\varphi}_\gamma^{e_i'}]^{\mathrm{T}}\bar{\boldsymbol{v}}^{e_i}\,\mathrm{d}\theta, + \int_{\omega_{i-1}}^{\omega_i}[((\alpha+\gamma)^2[A_4]\\ &+(\alpha+\gamma)[A_5]+[A_6])\boldsymbol{\varphi}_\gamma^{e_i}]^{\mathrm{T}}\bar{\boldsymbol{v}}^{e_i}\,\mathrm{d}\theta\\ &-\left\{[((\alpha+\gamma)[B_2]+[B_3])\boldsymbol{\varphi}_\gamma^{e_i}]^{\mathrm{T}}\bar{\boldsymbol{v}}^{e_i}\right\}|_{\omega_{i-1}}^{\omega_i},\end{aligned} \tag{41}$$

$$\begin{aligned}\mathscr{F}^\gamma(\boldsymbol{v}^{e_i}) = &-\int_{\omega_{i-1}}^{\omega_i}([A_7]\boldsymbol{\varphi}_{\gamma-1}^{e_i'})^{\mathrm{T}}\bar{\boldsymbol{v}}^{e_i}\,\mathrm{d}\theta - \int_{\omega_{i-1}}^{\omega_i}[((\alpha+\gamma-1)[A_8]\\ &+[A_9])\boldsymbol{\varphi}_{\gamma-1}^{e_i}]^{\mathrm{T}}\bar{\boldsymbol{v}}^{e_i}\,\mathrm{d}\theta\\ &-\varrho\int_{\omega_{i-1}}^{\omega_i}[([A_{10}])\boldsymbol{\varphi}_{\gamma-2}^{e_i}]^{\mathrm{T}}\bar{\boldsymbol{v}}^{e_i}\,\mathrm{d}\theta\\ &+\left\{([B_4]\boldsymbol{\varphi}_{\gamma-1}^{e_i})^{\mathrm{T}}\bar{\boldsymbol{v}}^{e_i}\right\}|_{\omega_{i-1}}^{\omega_i}.\end{aligned} \tag{42}$$

In the assembly procedure continuity of the displacement is enforced. The two surfaces $\theta = 0, \omega$ are therefore under traction free condition. In the case of Dirichlet boundary condition Sobolev space H^1 is replaced by $\overset{\circ}{H}{}^1 = \{\boldsymbol{v}|\boldsymbol{v}\in H^1, \boldsymbol{v}(\theta=0,\omega)=\boldsymbol{0}\}$.

4.2. p-FEMs for the solution of (40)

We apply p-FEMs for the solution of (40) similarly to Section 3.1. To this end $\boldsymbol{\varphi}_\gamma = (u_\gamma \quad v_\gamma \quad w_\gamma)^{\mathrm{T}} = [N]\boldsymbol{a}_\gamma$ and $\bar{\boldsymbol{v}} \overset{\text{def}}{=} [N]\boldsymbol{b}_\gamma$.

The resulting FE formulation is

$$\boldsymbol{a}_\gamma^{\mathrm{T}}[K^\gamma] = \boldsymbol{F}^{\gamma\mathrm{T}}, \tag{43}$$

where

$$\begin{aligned}[K^\gamma]^{e_i} = &-\left\{[N]^{\mathrm{T}}((\alpha+\gamma)[B_2]^{\mathrm{T}}+[B_3]^{\mathrm{T}})[N]\right\}|_{\omega_{i-1}}^{\omega_i}\\ &-\frac{2}{\omega^{e_i}}\int_{-1}^{1}[N']^{\mathrm{T}}[A_1]^{\mathrm{T}}[N']\mathrm{d}\xi\\ &+\int_{-1}^{1}[N']^{\mathrm{T}}((\alpha+\gamma)[A_2]^{\mathrm{T}}+[A_3]^{\mathrm{T}})[N]\mathrm{d}\xi\\ &+\frac{\omega^{e_i}}{2}\int_{-1}^{1}[N]^{\mathrm{T}}((\alpha+\gamma)^2[A_4]^{\mathrm{T}}+(\alpha+\gamma)[A_5]^{\mathrm{T}}+[A_6]^{\mathrm{T}})[N]\mathrm{d}\xi,\end{aligned}$$

$$\begin{aligned}\boldsymbol{F}^{\gamma e_i} = &\left\{\boldsymbol{a}_{\gamma-1}^{e_i T}[N]^{\mathrm{T}}[B_4]^{\mathrm{T}}[N]\right\}|_{\omega_{i-1}}^{\omega_i} - \int_{-1}^{1}\boldsymbol{a}_{\gamma-1}^{e_i T}[N']^{\mathrm{T}}[A_7]^{\mathrm{T}}[N]\mathrm{d}\xi\\ &-\frac{\omega^{e_i}}{2}\int_{-1}^{1}\boldsymbol{a}_{\gamma-1}^{e_i T}[N]^{\mathrm{T}}((\alpha+\gamma-1)[A_8]^{\mathrm{T}}+[A_9]^{\mathrm{T}})[N]\mathrm{d}\xi\\ &-\varrho\frac{\omega^{e_i}}{2}\int_{-1}^{1}\boldsymbol{a}_{\gamma-2}^{e_i T}[N]^{\mathrm{T}}([A_{10}]^{\mathrm{T}})[N]\mathrm{d}\xi.\end{aligned} \tag{44}$$

$[K^\gamma]$ are the assembled matrices formed of $[K^\gamma]^{e_i}$ and $\boldsymbol{F}^\gamma$ are the assembled vectors formed of $\boldsymbol{F}^{\gamma e_i}$. For clamped BCs $[B_2]|_0 = [B_2]|_\omega = [B_3]|_0 = [B_3]|_\omega = [0]$.

Substituting $\alpha = \alpha_\Re + i\alpha_\Im, \boldsymbol{a}_\gamma = \boldsymbol{a}_\gamma^\Re + \mathrm{i}\boldsymbol{a}_\gamma^\Im, \boldsymbol{a}_{\gamma-1} = \boldsymbol{a}_{\gamma-1}^\Re + \mathrm{i}\boldsymbol{a}_{\gamma-1}^\Im$ and $\boldsymbol{a}_{\gamma-2} = \boldsymbol{a}_{\gamma-2}^\Re + \mathrm{i}\boldsymbol{a}_{\gamma-2}^\Im$ into (44) we obtain the FE formulation:

$$\begin{pmatrix}\boldsymbol{a}_\gamma^\Re\\ \boldsymbol{a}_\gamma^\Im\end{pmatrix}^{\mathrm{T}}\begin{pmatrix}[K^\gamma]_\Re & [K^\gamma]_\Im\\ -[K^\gamma]_\Im & [K^\gamma]_\Re\end{pmatrix} = \begin{pmatrix}\boldsymbol{F}_\Re^\gamma\\ \boldsymbol{F}_\Im^\gamma\end{pmatrix}^{\mathrm{T}}, \tag{45}$$

where

$$\begin{aligned}[K^\gamma]_\Re^{e_i} = &-\left\{[N]^{\mathrm{T}}((\alpha_\Re+\gamma)[B_2]^{\mathrm{T}}+[B_3]^{\mathrm{T}})[N]\right\}|_{\omega_{i-1}}^{\omega_i}\\ &-\frac{2}{\omega^{e_i}}\int_{-1}^{1}[N']^{\mathrm{T}}[A_1]^{\mathrm{T}}[N']\mathrm{d}\xi\\ &+\int_{-1}^{1}[N']^{\mathrm{T}}((\alpha_\Re+\gamma)[A_2]^{\mathrm{T}}+[A_3]^{\mathrm{T}})[N]\mathrm{d}\xi\\ &+\frac{\omega^{e_i}}{2}\int_{-1}^{1}[N]^{\mathrm{T}}(((\alpha_\Re+\gamma)^2-\alpha_\Im^2)[A_4]^{\mathrm{T}}\\ &+(\alpha_\Re+\gamma)[A_5]^{\mathrm{T}}+[A_6]^{\mathrm{T}})[N]\mathrm{d}\xi,\end{aligned}$$

$$\begin{aligned}[K^\gamma]_\Im^{e_i} = &-\left\{[N]^{\mathrm{T}}(\alpha_\Im[B_2]^{\mathrm{T}})[N]\right\}|_{\omega_{i-1}}^{\omega_i} + \int_{-1}^{1}[N']^{\mathrm{T}}(\alpha_\Im[A_2]^{\mathrm{T}})[N]\mathrm{d}\xi\\ &+\frac{\omega^{e_i}}{2}\int_{-1}^{1}[N]^{\mathrm{T}}(2(\alpha_\Re+\gamma)\alpha_\Im[A_4]^{\mathrm{T}}+\alpha_\Im[A_5]^{\mathrm{T}})[N]\mathrm{d}\xi,\end{aligned}$$

$$\begin{aligned}\boldsymbol{F}_\Re^{\gamma e_i} = &\left\{\boldsymbol{a}_{\gamma-1}^{\Re e_i T}[N]^{\mathrm{T}}[B_4]^{\mathrm{T}}[N]\right\}|_{\omega_{i-1}}^{\omega_i} - \int_{-1}^{1}\boldsymbol{a}_{\gamma-1}^{\Re e_i T}[N']^{\mathrm{T}}[A_7]^{\mathrm{T}}[N]\mathrm{d}\xi\\ &-\frac{\omega^{e_i}}{2}\int_{-1}^{1}((\alpha_\Re+\gamma-1)\boldsymbol{a}_{\gamma-1}^{\Re e_i}-\alpha_\Im\boldsymbol{a}_{\gamma-1}^{\Im e_i})^{\mathrm{T}}[N]^{\mathrm{T}}[A_8]^{\mathrm{T}}[N]\mathrm{d}\xi\\ &-\frac{\omega^{e_i}}{2}\int_{-1}^{1}\boldsymbol{a}_{\gamma-1}^{\Re e_i T}[N]^{\mathrm{T}}[A_9]^{\mathrm{T}}[N]\mathrm{d}\xi-\frac{\omega}{2}\int_{-1}^{1}\boldsymbol{a}_{\gamma-2}^{\Re e_i T}[N]^{\mathrm{T}}[A_{10}]^{\mathrm{T}}[N]\mathrm{d}\xi,\end{aligned}$$

$$\begin{aligned}\boldsymbol{F}_\Im^{\gamma e_i} = &\left\{\boldsymbol{a}_{\gamma-1}^{\Im e_i T}[N]^{\mathrm{T}}[B_4]^{\mathrm{T}}[N]\right\}|_{\omega_{i-1}}^{\omega_i} - \int_{-1}^{1}\boldsymbol{a}_{\gamma-1}^{\Im e_i T}[N']^{\mathrm{T}}[A_7]^{\mathrm{T}}[N]\mathrm{d}\xi\\ &-\frac{\omega^{e_i}}{2}\int_{-1}^{1}(\alpha_\Im\boldsymbol{a}_{\gamma-1}^{\Re e_i}+(\alpha_\Re+\gamma-1)\boldsymbol{a}_{\gamma-1}^{\Im e_i})^{\mathrm{T}}[N]^{\mathrm{T}}[A_8]^{\mathrm{T}}[N]\mathrm{d}\xi\\ &-\frac{\omega^{e_i}}{2}\int_{-1}^{1}\boldsymbol{a}_{\gamma-1}^{\Im e_i T}[N]^{\mathrm{T}}[A_9]^{\mathrm{T}}[N]\mathrm{d}\xi\\ &-\frac{\omega^{e_i}}{2}\int_{-1}^{1}\boldsymbol{a}_{\gamma-2}^{\Im e_i T}[N]^{\mathrm{T}}[A_{10}]^{\mathrm{T}}[N]\mathrm{d}\xi,\end{aligned} \tag{46}$$

$[K^\gamma]_\Re, [K^\gamma]_\Im$ are the assembled matrices from $[K^\gamma]_\Re^{e_i}$ and $[K^\gamma]_\Im^{e_i}$. $\boldsymbol{F}_\Re^\gamma, \boldsymbol{F}_\Im^\gamma$ are the assembled vectors from $\boldsymbol{F}_\Re^{\gamma e_i}$ and $\boldsymbol{F}_\Im^{\gamma e_i}$.

4.3. Difficulties in computing shadows and remedies for several pathological cases

There are several pathological cases, among which one is of major importance being the cracked case, where the numerical methods presented fail, and remedies are to be implemented. These pathological cases occur when $\alpha_i = \alpha_j - n$ for n being an integer. For a cracked configuration for example, $\alpha_1 = \alpha_2 = \alpha_3 = 1/2, \alpha_4 = \alpha_5 = \alpha_6 = 1$, $\alpha_7 = \alpha_8 = \alpha_9 = 3/2$, etc. In this case consider for example the first shadow function associated with $\alpha_1 = 1/2$ – which has to satisfy the *non-homogeneous* ODE $(9)_2$:

$$[\mathscr{M}_0]\boldsymbol{\varphi}_1^{(\alpha_1)} = \left([A_1]\partial_\theta^2 + \left(\frac{3}{2}[A_2] + [A_3]\right)\partial_\theta + \left(\left(\frac{3}{2}\right)^2[A_4] + \frac{3}{2}[A_5] + [A_6]\right)\right)\boldsymbol{\varphi}_1^{(\alpha_1)} = -[\mathscr{M}_1]\boldsymbol{\varphi}_0^{(\alpha_1)}. \tag{47}$$

Formally, the solution (47) may be obtained by the inverse of the operator $[\mathscr{M}_0]$ applied to the RHS. Practically, when FE discretization is applied the operator $[\mathscr{M}_0]$ results in the matrix $[K^1]$ that has to be inverted and must not be singular. This is equivalent to requiring a particular solution without the homogeneous part of the solution. However, the LHS of (47) is exactly the ODE for the computation of $\boldsymbol{\varphi}_0^{(\alpha_1+1)}$, only that for $\boldsymbol{\varphi}_0^{(\alpha_1+1)}$ the ODE is *homegeneous*:

$$[\mathscr{M}_0]\boldsymbol{\varphi}_0^{(\alpha_1+1)} = \left([A_1]\partial_\theta^2 + \left(\frac{3}{2}[A_2] + [A_3]\right)\partial_\theta + \left(\left(\frac{3}{2}\right)^2[A_4] + \frac{3}{2}[A_5] + [A_6]\right)\right)\boldsymbol{\varphi}_1^{(\alpha_1)} = \mathbf{0}. \tag{48}$$

In the continuum case (i.e. theoretically as the number of degrees of freedom tend to infinity) $[K^1]$ is singular and may not be inverted. Practically, because the eigen-values are computed numerically, the larger the eigen-value the worse is the approximation, so $[K^1]$ is not identically singular, but ill-conditioned, and as the polynomial degree is increased (resulting in better approximation of eigen-values) the more ill-conditioned $[K^1]$ becomes. Of course this situation occurs with any of the dual shadow functions computed numerically.

The remedy to this problem is achieved if one notices that only a particular solution of (47) is sought, therefore a constraint can be added that the sought solution is orthogonal to the homogeneous solution for the operator $[\mathscr{M}_0]$. Practically, in the FE formulation one has to enforce the additional condition that the scalar product between $\boldsymbol{a}_1^{(\alpha_1)}$ and $\bar{\boldsymbol{a}}_0^{(\alpha_1+1)}$, for example, is zero. Or in general, we add scalar product between $\boldsymbol{a}_\gamma^{(\alpha_i)}$ and $\bar{\boldsymbol{a}}_0^{(\alpha_j)}$ where $\alpha_j = \alpha_i + \gamma$ (if α_j exist) to ensure that $\boldsymbol{a}_\gamma^{(\alpha_i)}$ is not $\boldsymbol{a}_0^{(\alpha_j)}, \bar{\boldsymbol{a}}_0^{(\alpha_j)}$ dependent.

The system (45) for these pathological cases becomes therefore:

$$\underbrace{\begin{pmatrix} \boldsymbol{a}_\gamma^{\Re(\alpha_i)} \\ \boldsymbol{a}_\gamma^{\Im(\alpha_i)} \end{pmatrix}^{\mathrm{T}}}_{(1\times S)} \underbrace{\begin{pmatrix} [K^\gamma]_\Re & [K^\gamma]_\Im & \boldsymbol{a}_0^{\Re(\alpha_j)} & -\boldsymbol{a}_0^{\Im(\alpha_j)} \\ -[K^\gamma]_\Im & [K^\gamma]_\Re & \boldsymbol{a}_0^{\Im(\alpha_j)} & \boldsymbol{a}_0^{\Re(\alpha_j)} \end{pmatrix}}_{(S\times(S+2))} = \underbrace{\begin{pmatrix} \boldsymbol{F}_\Re^\gamma \\ \boldsymbol{F}_\Im^\gamma \\ 0 \\ 0 \end{pmatrix}^{\mathrm{T}}}_{(1\times(S+2))}, \tag{49}$$

where $S = 3pQ + 3$, Q is the number of elements. Since system (49) is now over-determined system of equations, we use least squares solution to determine $\boldsymbol{a}_\gamma^{\Re(\alpha_i)}$ and $\boldsymbol{a}_\gamma^{\Im(\alpha_i)}$.

To demonstrate the pathological case discussed, as an example, we compute the eigen-pairs and first two shadow functions of an orthotropic bi-material cracked domain shown in Fig. 2. Both materials are made of the same high-modulus graphite-epoxy system with different fiber orientation. Referring to the principle direction of the fibers, the material properties are:

$$E_L = 1.38\times10^5 \text{ MPa} \quad E_T = E_z = 1.45\times10^4 \text{ MPa}$$
$$G_{LT} = G_{Lz} = G_{Tz} = 0.586\times10^4 \text{ MPa}, \quad \nu_{LT} = \nu_{Lz} = \nu_{Tz} = 0.21, \tag{50}$$

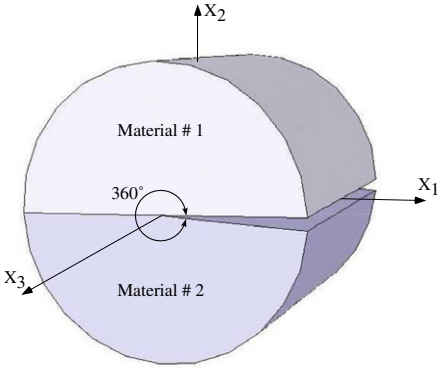

Fig. 2. Bi-material cracked domain.

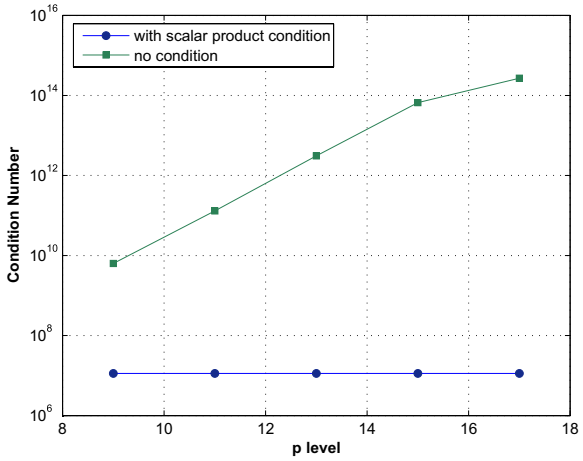

Fig. 3. Condition number of $[K^2]$ associated with $\boldsymbol{\varphi}_2^{(\alpha_{1,2})}, \alpha_{1,2} = 0.5 \pm$ i0.0510612.

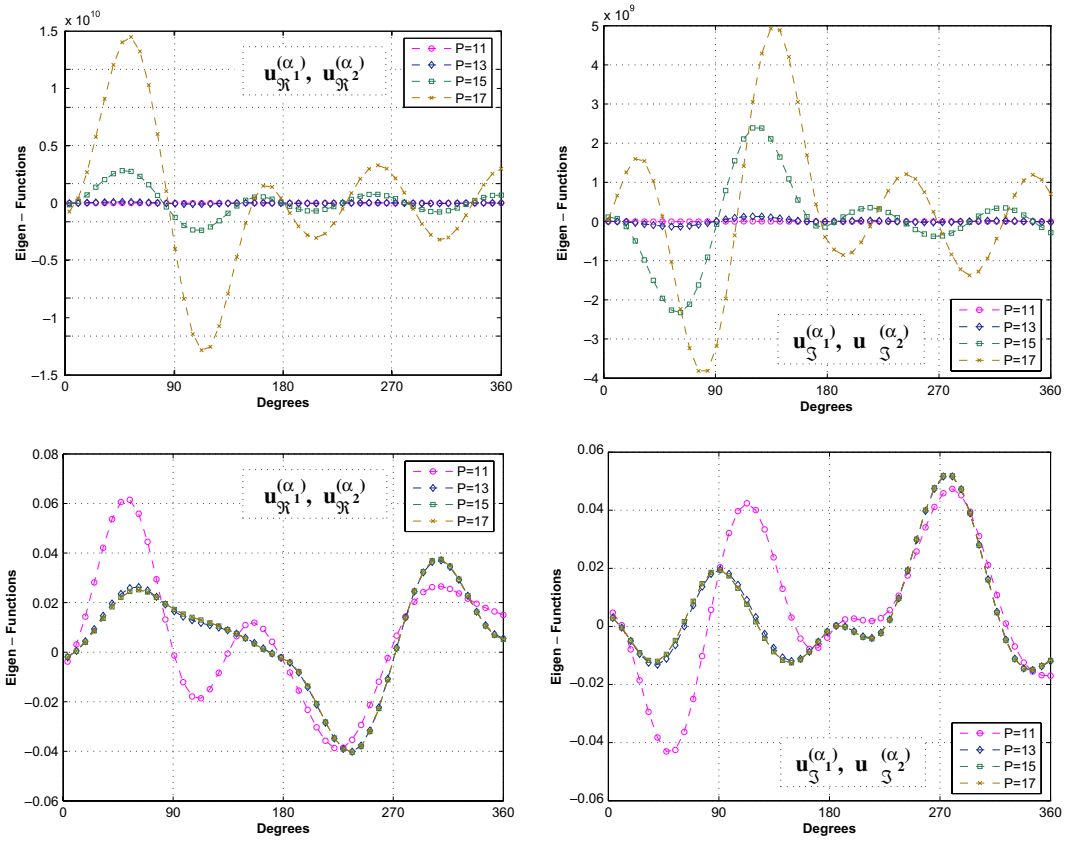

Fig. 4. The functions u_2 associated with $\varphi_2^{(\alpha_{1,2})}, \alpha_{1,2} = 0.5 \pm 0.0510612$, computed using 8 elements without (top) and with (bottom) the scalar product condition.

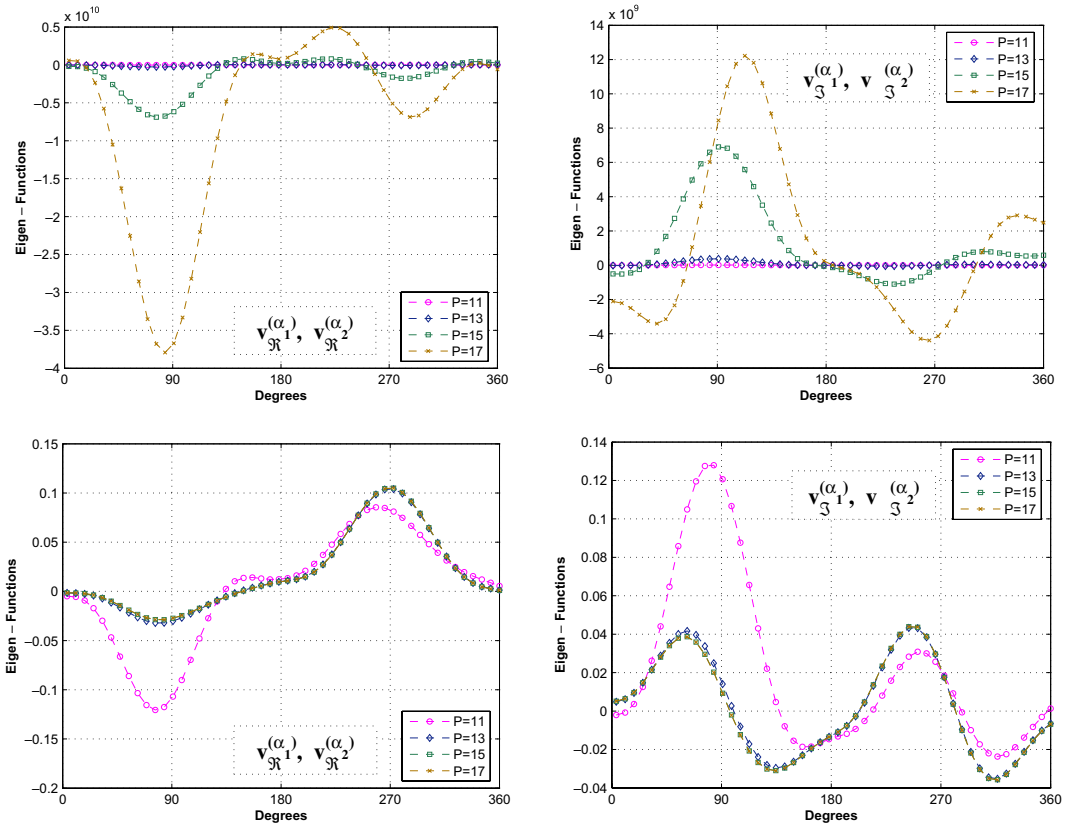

Fig. 5. The functions v_2 of $\varphi_2^{(\alpha_{1,2})}, \alpha_{1,2} = 0.5 \pm 0.0510612$, computed using 8 elements without (top) and with (bottom) the scalar product condition.

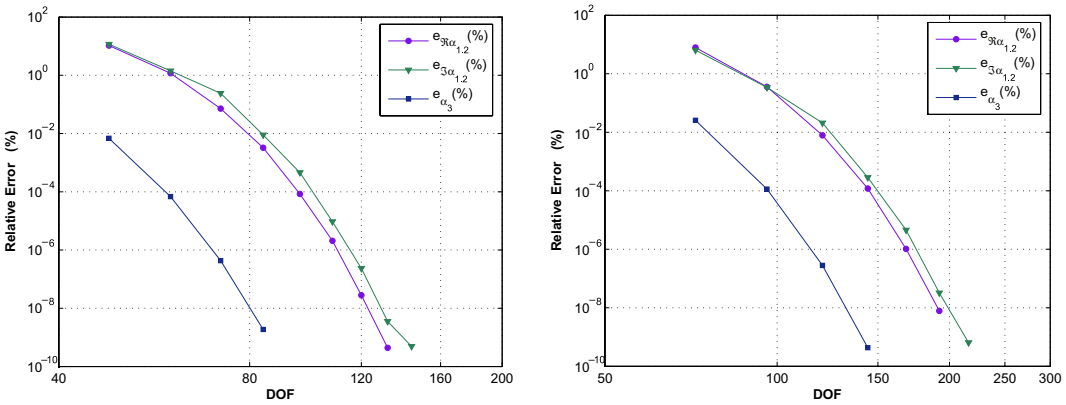

Fig. 6. Relative error (percentage) in eigen-values $\alpha_1^{FE}, \alpha_2^{FE}, \alpha_3^{FE}$, for example A, computed by 2 (left) and 4 (right) elements.

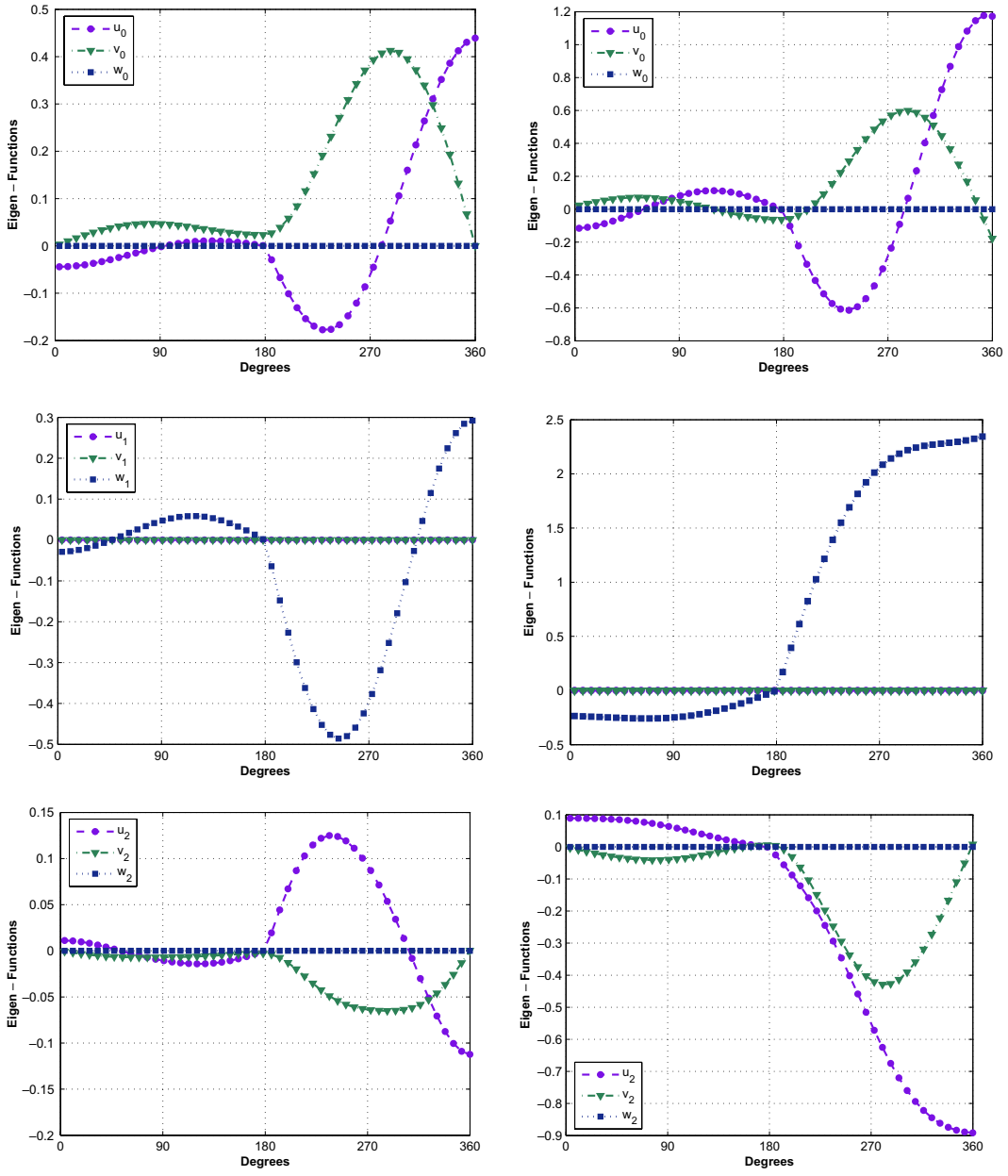

Fig. 7. The real part of the eigen-functions (left) and dual eigen-functions (right) associated with $\alpha_{1,2} = 0.5 \pm i0.075812$, of example A, computed by 4 elements, $p = 6$.

where the subscripts L, T, z refer to fiber, transverse and thickness direction of individual material. The orientation of fibers of the upper material (Material # 1) is in x_1 direction whereas the orientation at the lower material (Material # 2) is in x_3 direction. The first three eigen-values for this example problem, computed using 8 elements at $p = 15$ are:

$$\alpha_{1,2} = 0.5 \pm \mathrm{i}0.05106124425, \qquad \alpha_3 = 0.5. \tag{51}$$

In this example also the eigen-values $\alpha = 2.5 \pm \mathrm{i}0.05106124425$, $(\alpha = \alpha_{1,2} + 2)$ which causes the $[K^2]$ matrix of $\boldsymbol{\varphi}_2^{(\alpha_1)}$ to be singular. Fig. 3 shows the condition number of the matrix $[K^2]$ associated with $\boldsymbol{\varphi}_2^{(\alpha_1)}$, computed using increasing p-level. It may be noticed that the condition number of $[K^2]$ increases continuously as p is increased. The condition number of $[K^2]$ after incorporating the constrain of the scalar product remains constant.

The functions u_2 and v_2 of $\boldsymbol{\varphi}_2^{(\alpha_{1,2})}$ computed with and without the scalar product condition are presented in Figs. 4 and 5, respectively.

It is visible from Figs. 4 and 5, that the functions computed without any additional condition are scattered whereas the functions computed using the scalar product condition converge.

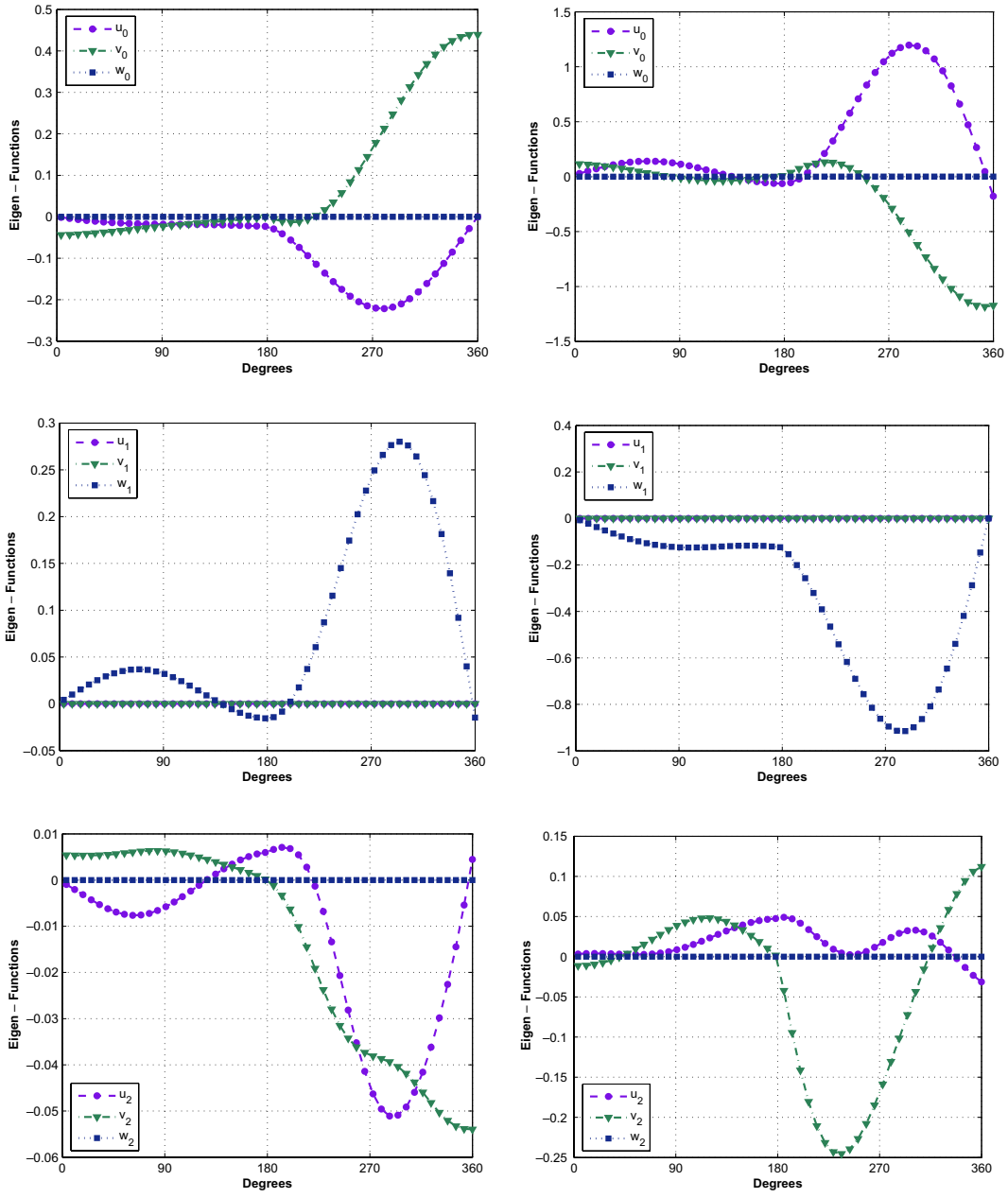

Fig. 8. The image part of the eigen-functions (left) and dual eigen-functions (right) associated with $\alpha_{1,2} = 0.5 \pm \mathrm{i}0.075812$ of example A, computed by four elements, $p = 6$.

5. Extracting complex edge stress intensity function by the quasi-dual function method (QDFM)

The QDFM was theoretically introduced in [4], applied for the extraction of edge stress intensity functions (ESIF) in isotropic domains using high-order finite elements in [12] and extended to anisotropic domains in [11]. Herein, it's extension to complex ESIFs and multi-material interfaces is provided. Assume the ESIF $A_i(x_3)$ is of interest. For its extraction the *quasidual*-singular function $\mathbf{K}_m^{(\alpha_i)}[B]$ is constructed where m is a natural integer called the *order* of the quasidual function, and $B(x_3)$ is a function, provided in the sequel, called *extraction polynomial*. $\mathbf{K}_m^{(\alpha_i)}[B]$ is characterized by the number of dual singular functions m needed for its construction and the extraction polynomial B:

$$\mathbf{K}_m^{(\alpha_i)}[B] \stackrel{\text{def}}{=} \sum_{j=0}^{m} \partial_3^j B(x_3) \boldsymbol{\Psi}_j^{(\alpha_i)}. \tag{52}$$

A scalar product of $A_i(x_3)$ with $B(x_3)$ on $\mathscr{E}$ can be extracted with the help of the *anti-symmetric* boundary integral $J[R]$, over the cylindrical surface Γ_R (2).

$$J[R](\tilde{\boldsymbol{u}}, \mathbf{K}_m^{(\alpha_i)}[B]) \stackrel{\text{def}}{=} \int_I \int_0^{\omega} (\boldsymbol{T}^{\Gamma_R}\tilde{\boldsymbol{u}} \cdot \mathbf{K}_m^{(\alpha_i)}[B] - \tilde{\boldsymbol{u}} \cdot \boldsymbol{T}^{\Gamma_R}\mathbf{K}_m^{(\alpha_i)}[B])|_{r=R} R \,\mathrm{d}\theta \,\mathrm{d}x_3, \tag{53}$$

where $I \equiv \mathscr{E}$ (the edge) along x_3 axis (Fig. 1) and $\boldsymbol{T}^{\Gamma_R}$ is the radial Neumann trace operator presented in (30). Note that

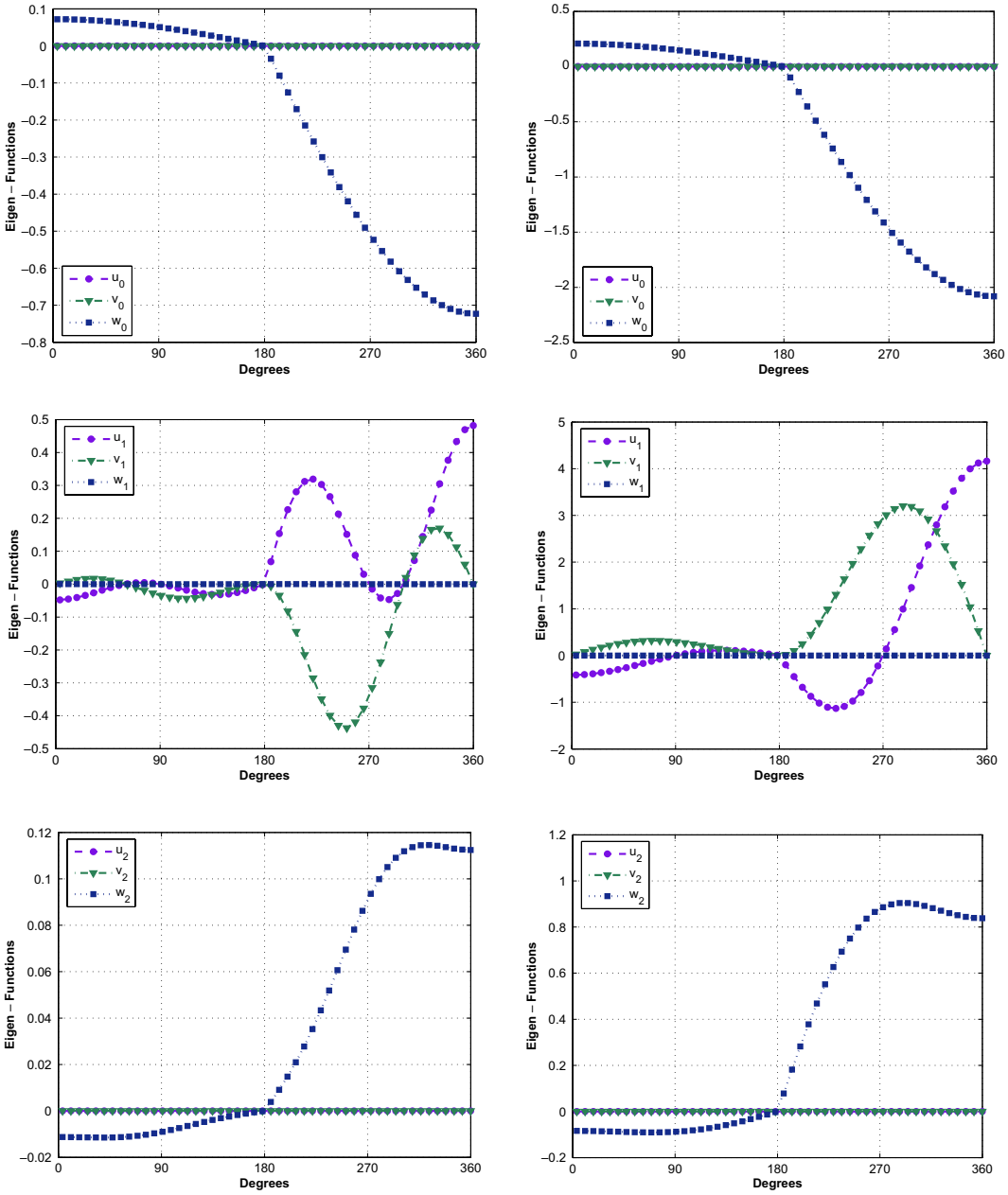

Fig. 9. Eigen-functions (left) and dual eigen-functions (right) associated with $\alpha_3 = 0.5$ of example A, computed by four elements, $p = 6$.

$J[R]$ in (53) is unrelated to the classical J-integral [9], but rather it is an extension of the dual singular function method [3] to 3-D domains.

With the above definitions we have the following theorem [4]:

Theorem 1. *Take* $B(x_3)$ *such that*

$$\partial_3^j B(x_3) = 0 \quad \text{for} \quad j = 0, \ldots, m-1 \ \text{ on } \partial I \tag{54}$$

then, if the ESIFs A_i *in the expansion* (1) *are smooth enough*:

$$J[R](\tilde{\boldsymbol{u}}, \mathbf{K}_m^{(\alpha_i)}[B]) = \int_I A_i(x_3)B(x_3)\mathrm{d}x_3 + \mathcal{O}(R^{\Re(\alpha_1)-\Re(\alpha_i)+m+1}), \quad \text{as} \quad R \to 0. \tag{55}$$

Here $\Re(\alpha_1)$ *is the smallest of all positive eigen-values* α_i.

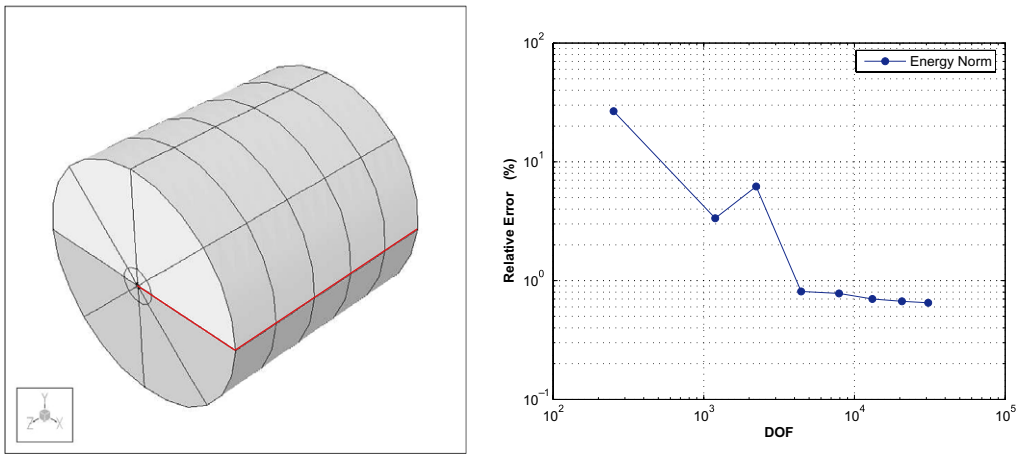

Fig. 10. (left) The p-FEM model of example A, having 160 elements. (right) Convergence rate of the relative error in the energy norm.

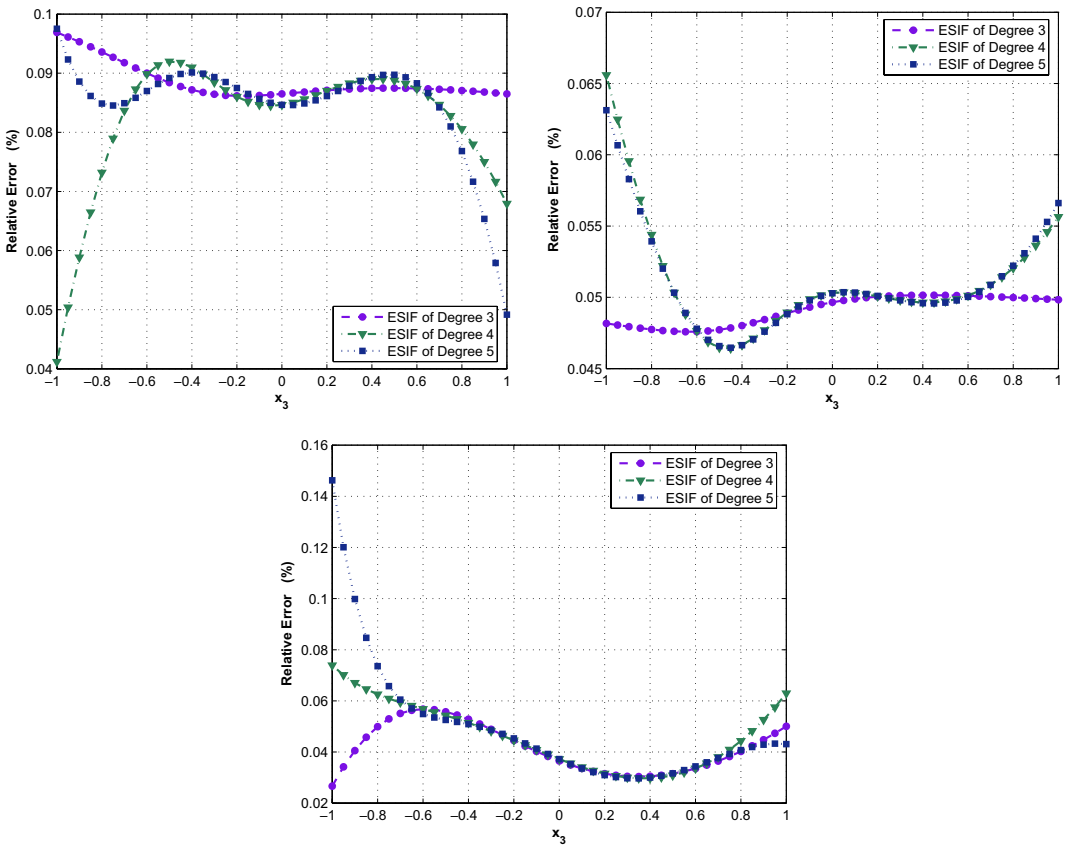

Fig. 11. Relative error of extracted ESIF. Eigen-functions computed using $p = 6$ and 4 element model, ESIF computed using $B^{(k)}$ with $k = 3, 4, 5$ and $R = 0.05$ for Example A.

In the case of complex eigen-values $A_i(x_3) = A_i^{\Re}(x_3) + \imath A_i^{\Im}(x_3)$ and $B(x_3) = B^{\Re}(x_3) + \imath B^{\Im}(x_3)$. Choosing $m = 2$ we have in (55) $\mathcal{O}(R^{\Re(\alpha_1)-\Re(\alpha_i)+3})$. Theorem 1 allows a precise determination of $\int_I A_i(x_3)B(x_3)\mathrm{d}x_3$ by computing (55) for two or three R values as $R \to 0$. The extraction functions $B(x_3)$ are based on Jacobi polynomials [12] so that if $A_i(x_3)$ is a polynomial of degree N, it is expanded as a linear combination of Jacobi polynomials. For the functions $B(x_3)$ we chose them to satisfy $\partial_3^j B(x_3) = 0$ for $j = 0, 1, 2, 3$, more than required in (54) (see reasoning in [12]). The family of extraction polynomials is constructed by:

$$B^{\Re(k)}(x_3) = B^{\Im(k)}(x_3) = (1 - x_3^2)^4 \frac{\mathscr{J}_4^{(k)}(x_3)}{h_k},$$
$$h_k = \frac{2^9(k+4)!(k+4)!}{(2k+9)(k+8)!}, \tag{56}$$

where $\mathscr{J}_4^{(k)}(x_3)$ is the Jacobi polynomial of degree k and order 4. If we take an approximation of $A_i(x_3)$ as a polynomial of Nth order, being a linear combination of Jacobi polynomials:

$$A_i(x_3) = A_i^{\Re}(x_3) + iA_i^{\Im}(x_3),$$
$$\begin{cases} A_i^{\Re}(x_3) = \tilde{a}_0^{\Re}\mathscr{J}_4^{(0)}(x_3) + \tilde{a}_1^{\Re}\mathscr{J}_4^{(1)}(x_3) + \cdots + \tilde{a}_N^{\Re}\mathscr{J}_4^{(N)}(x_3) \\ A_i^{\Im}(x_3) = \tilde{a}_0^{\Im}\mathscr{J}_4^{(0)}(x_3) + \tilde{a}_1^{\Im}\mathscr{J}_4^{(1)}(x_3) + \cdots + \tilde{a}_N^{\Im}\mathscr{J}_4^{(N)}(x_3) \end{cases} \tag{57}$$

then we can obtain the coefficients $\tilde{a}_i$ directly by applying Theorem 1 with the different extraction polynomials:

$$\int_{-1}^{1} A_i(x_3)B^{(k)}(x_3)\mathrm{d}x_3 = J^{\Re(k)} + iJ^{\Im(k)}, \quad k = 0, 1, \ldots, N. \tag{58}$$

where

$$J^{\Re(k)} = \int_{-1}^{1} (A_i^{\Re}(x_3)B^{\Re(k)}(x_3) - A_i^{\Im}(x_3)B^{\Im(k)}(x_3))\mathrm{d}x_3$$
$$J^{\Im(k)} = \int_{-1}^{1} (A_i^{\Re}(x_3)B^{\Im(k)}(x_3) + A_i^{\Im}(x_3)B^{\Re(k)}(x_3))\mathrm{d}x_3 \tag{59}$$

and

$$\tilde{a}_k^{\Re} = \frac{J^{\Re(k)} + J^{\Im(k)}}{2}, \quad \tilde{a}_k^{\Im} = \frac{-J^{\Re(k)} + J^{\Im(k)}}{2}. \tag{60}$$

In the view of (55), the $J[R]$ integral evaluated for the quasi-dual functions $K_m^{(\alpha_i)}[B^{(k)}], k = 0, 1, \ldots, N$ provides approximations of the coefficients $\tilde{a}_k$. Note that the polynomial degree is the superscript k. Of course, in general $A_i(x_3)$ is an unknown function and we only find a projection of it into spaces of polynomials. It is expected that as we increase the polynomial space, the approximation is progressively better.

The increase of the polynomial space in which $A_i(x_3)$ is projected is acheived by the computation of (55) for $k = N + 1$. This way: $A^{\text{new}}(x_3) = A^{\text{previous}}(x_3) + \tilde{a}_{N+1}\mathscr{J}_{N+1}(x_3)$.

Because the exact solution $\tilde{\boldsymbol{u}}$ is in general unknown one may use finite element methods and obtain $\tilde{\boldsymbol{u}}_{\text{FE}}$ instead, to be used in (53), and the integral being then computed by a Gaussian quadrature. The quantities $\tilde{\boldsymbol{u}}_{\text{FE}}$ and $\boldsymbol{T}^{\Gamma_R}\tilde{\boldsymbol{u}}_{\text{FE}}$ are computed numerically from the FE model of the entire domain FE, whereas $\mathbf{K}_2^{(\alpha_i)}[B^{(k)}]$ and $\boldsymbol{T}^{\Gamma_R}\mathbf{K}_2^{(\alpha_i)}[B^{(k)}]$ are computed numerically after computing by p-FEMs the dual and shadow functions $\boldsymbol{\psi}_0^{\text{FE}}, \boldsymbol{\psi}_1^{\text{FE}}$ and $\boldsymbol{\psi}_2^{\text{FE}}$ in Sections 3 and 4.

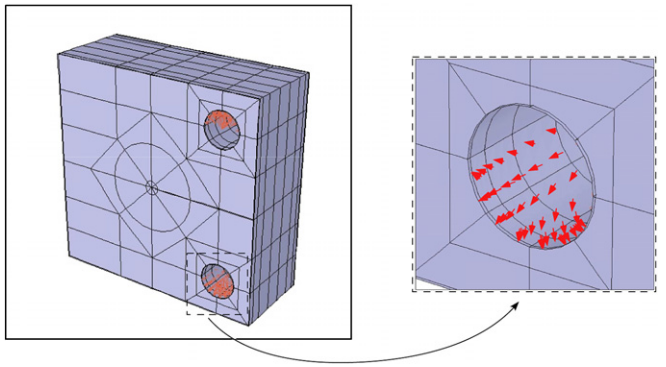

Fig. 13. The p-FEM model of the CTS with a constant loading in x_3 direction (the loading at the upper hole is as in the shown lower hole, in the opposite direction).

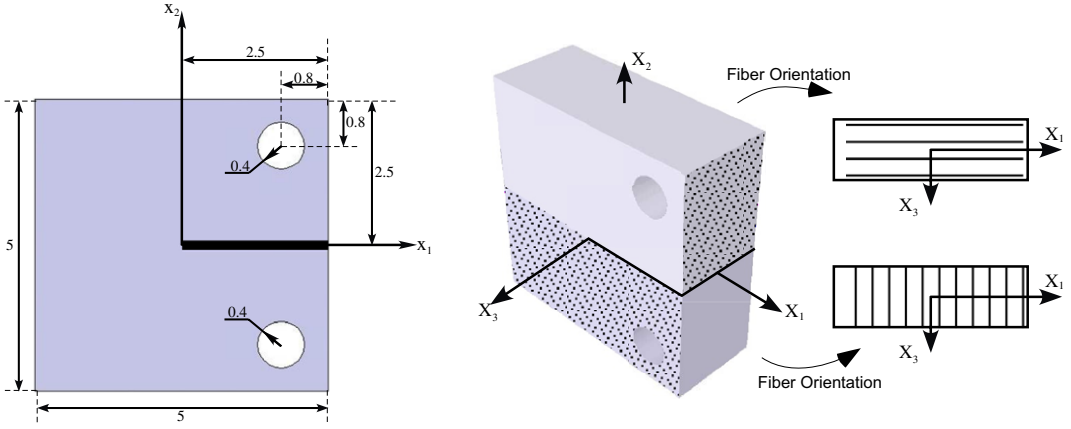

Fig. 12. Dimensions of CTS. The thickness of the specimen is 2 ranging from $-1 < x_3 < 1$.

6. Numerical examples

To demonstrate the accuracy of the proposed methods two example problems are considered herein. The first is a crack at a bi-material interface between two isotropic materials for which semi-analytical solutions are known thus the accuracy of the numerical results can be evaluated.

The second example problem is a crack in a compact test specimen at an interface of two anisotropic materials. Although the loading is perpendicular to the crack face, because of the anisotropy of the materials all three modes are exited.

6.1. Example A – crack at the interface of two isotropic materials

Consider a bi-material interface which is composed of two homogeneous materials (Fig. 2). The two materials are isotropic, both having Poisson ratio of $\nu = 0.3$, the Young modules of the upper material (material # 1) is $E = 10$ and of the lower material (material # 2) is $E = 1$. This example was chosen to present the performance of the method for cases of complex eigen-values. The exact first three eigen-values for this example problem, as reported in [10], are:

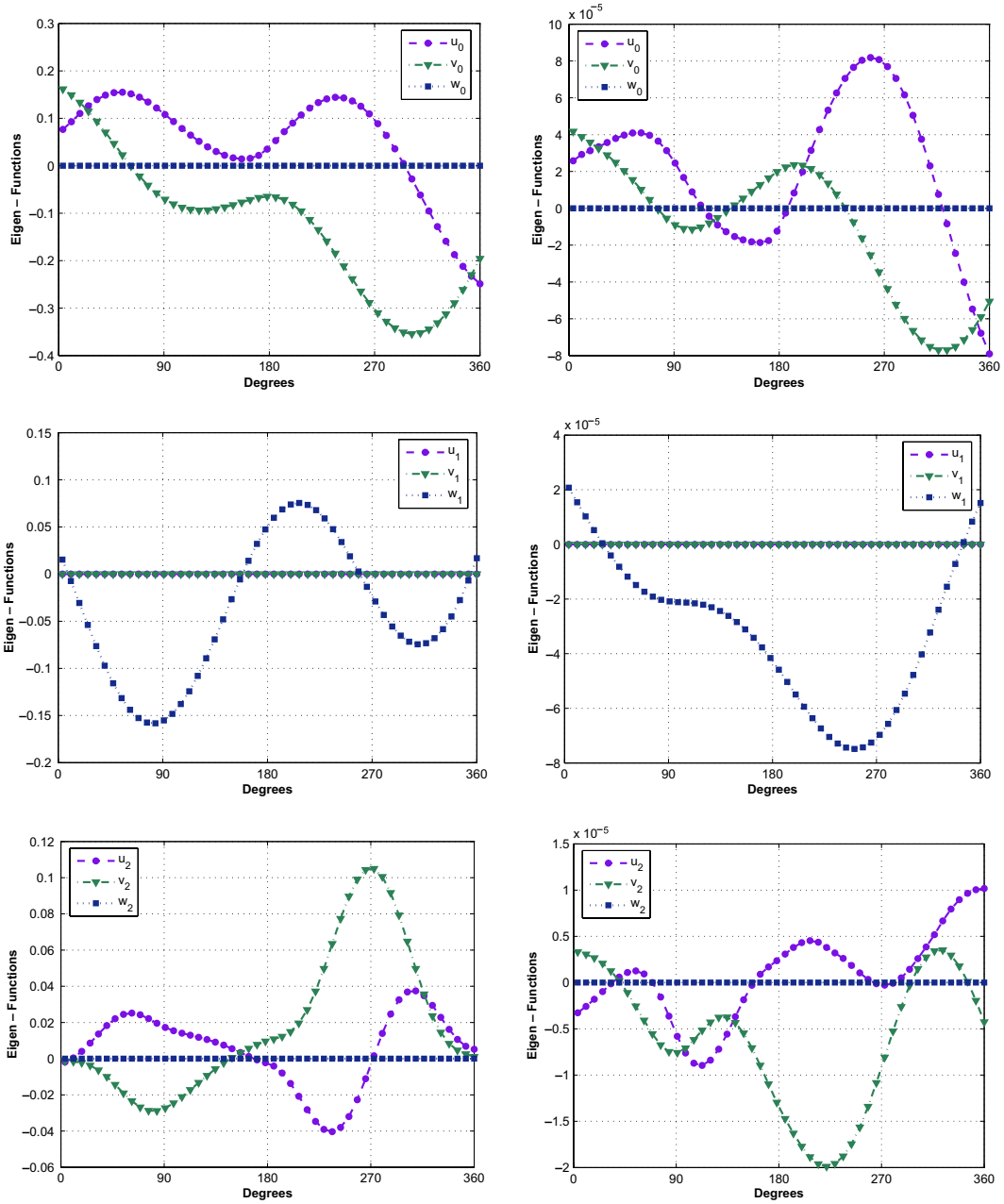

Fig. 14. Real part of the eigen-functions (left) and dual eigen-functions (right) associated with $\alpha_{1,2} = 0.5 \pm 0.0510612$, computed by 8 elements, $p = 15$.

$$\alpha_{1,2} = 0.5 \pm i0.07581177769, \quad \alpha_3 = 0.5. \tag{61}$$

The relative error in percentage in the first three eigen-values computed using 2 and 4 elements is shown in Fig. 6. For the first complex eigen-value the relative error is split into real and imaginary parts:

$$e_{\Re\alpha_{1,2}} = 100\frac{\Re(\alpha_{1,2}) - \Re(\alpha_{1,2}^{\mathrm{FE}})}{\Re(\alpha_{1,2})},$$
$$e_{\Im\alpha_{1,2}} = 100\frac{\Im(\alpha_{1,2}) - \Im(\alpha_{1,2}^{\mathrm{FE}})}{\Im(\alpha_{1,2})}. \tag{62}$$

The eigen-functions, duals and shadows associated with the first three eigen-values are presented in Figs. 7–9 computed using 4 elements, $p = 6$.

Obtaining the eigen-pairs and shadows for the first three eigen-values, we choose the ESIF to be, for example a polynomial of order 2. Thus, the solution is:

$$\begin{aligned}\tilde{\boldsymbol{u}} = {} & A_1(x_3)r^{\alpha_1}\boldsymbol{\varphi}_0^{(\alpha_1)}(\theta) + \partial_3 A_1(x_3)r^{\alpha_1+1}\boldsymbol{\varphi}_1^{(\alpha_1)}(\theta) \\ & + \partial_3^2 A_1(x_3)r^{\alpha_1+2}\boldsymbol{\varphi}_2^{(\alpha_1)}(\theta) + A_2(x_3)r^{\alpha_2}\boldsymbol{\varphi}_0^{(\alpha_2)}(\theta) \\ & + \partial_3 A_2(x_3)r^{\alpha_2+1}\boldsymbol{\varphi}_1^{(\alpha_2)}(\theta) + \partial_3^2 A_2(x_3)r^{\alpha_2+2}\boldsymbol{\varphi}_2^{(\alpha_2)}(\theta) \\ & + A_3(x_3)r^{\alpha_3}\boldsymbol{\varphi}_0^{(\alpha_3)}(\theta) + \partial_3 A_3(x_3)r^{\alpha_3+1}\boldsymbol{\varphi}_1^{(\alpha_3)}(\theta) \\ & + \partial_3^2 A_3(x_3)r^{\alpha_3+2}\boldsymbol{\varphi}_2^{(\alpha_3)}(\theta).\end{aligned} \tag{63}$$

Note that the eigen-pairs and shadows of example A are obtained numerically and therefore (63) represents an approximation of the exact solution only.

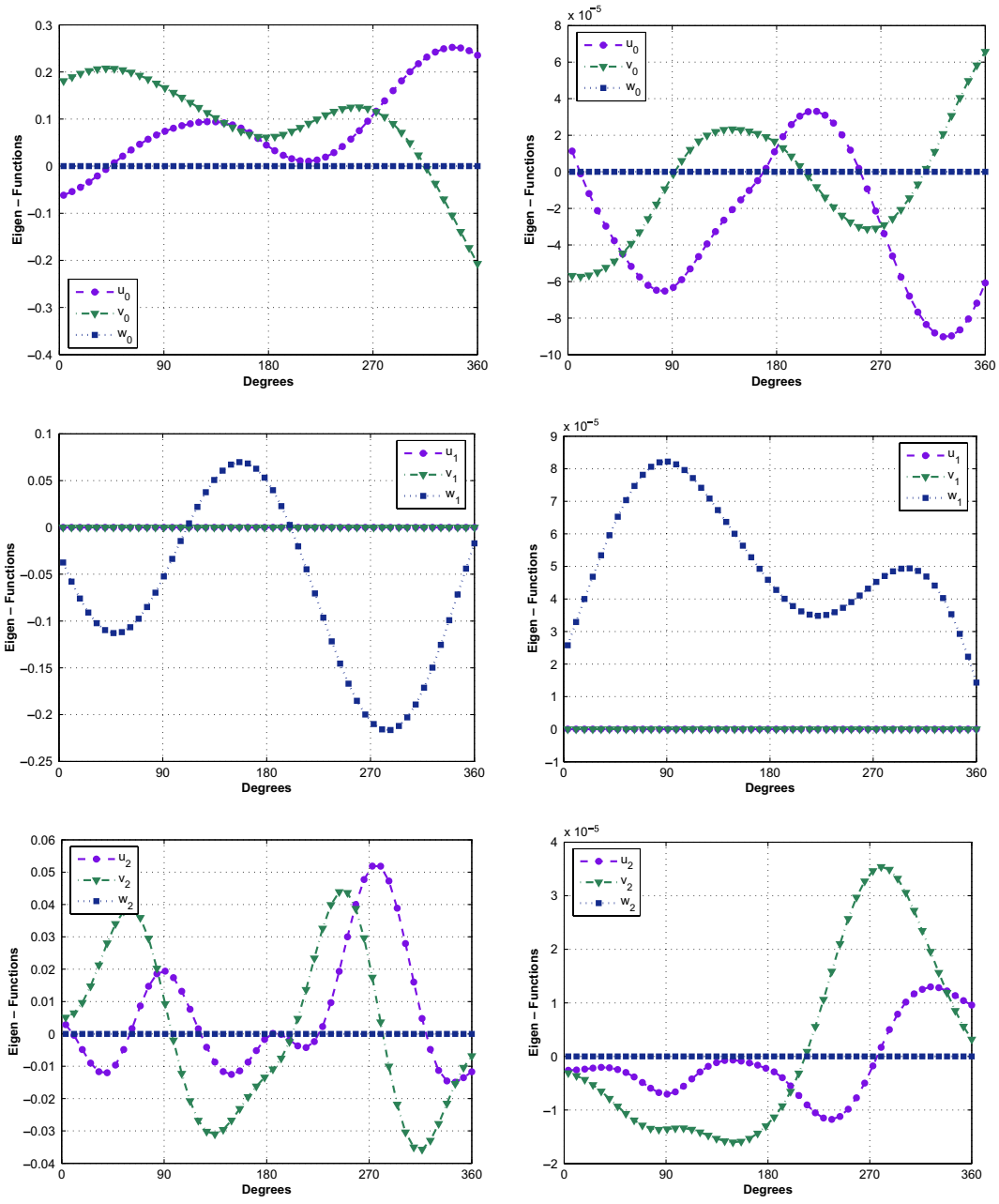

Fig. 15. Imaginary part of the eigen-functions (left) and dual eigen-functions (right) associated with $\alpha_{1,2} = 0.5 \pm 0.0510612$, computed by 8 elements, $p = 15$.

For example, consider the following exact ESIFs (polynomials of order 3):

$$A_{1,2}^{Ex}(x_3) = (3 + 4x_3 + 5x_3^2) \pm \mathrm{i}(2 + 3x_3 + 4x_3^2),$$
$$A_3^{Ex}(x_3) = 5 + 4x_3 + 2x_3^2. \tag{64}$$

If we prescribe on a traction free cracked domain Dirichlet boundary conditions according to (63) and (64), the exact solution at each r, θ, x_3 is as (63). Consider a 3-D domain as shown in Fig. 1 with $\omega = 2\pi$. The domain is discretized by using a p-FE mesh, with geometrical progression towards the singular edge with a factor of 0.15, having 4 layers of elements. In the x_3 direction, a uniform discretization using 5 elements has been adopted. In Fig. 10, we present the mesh used for the cracked domain and the convergence rate of the relative error in the energy norm.

We specify on the entire boundary $\partial\Omega$ Dirichlet boundary conditions according to (63). Therefore the exact solution at any point $\boldsymbol{x} \equiv (r, \theta, x_3)$ should be (63).

When $J[R]$ is computed with the quasi-dual function $\mathbf{K}_2^{(\alpha_i)}$ and $B^{(k)}(x_3)$ we expect to obtain, according to (55), (57) and (60) the coefficients $\tilde{a}_k^{\Re(\alpha_i)}, \tilde{a}_k^{\Im(\alpha_i)}$ for complex eigen-values or $\tilde{a}_k^{(\alpha_i)}$ for real eigen-values.

The ESIF is then easily represented by a linear combination of the Jacobi polynomials in (57). We extract the ESIFs at $R = 0.05$ by using the *numerically computed* dual eigen-pairs and their shadows with $K_2^{(\alpha_i)}[B^{(k)}]$.

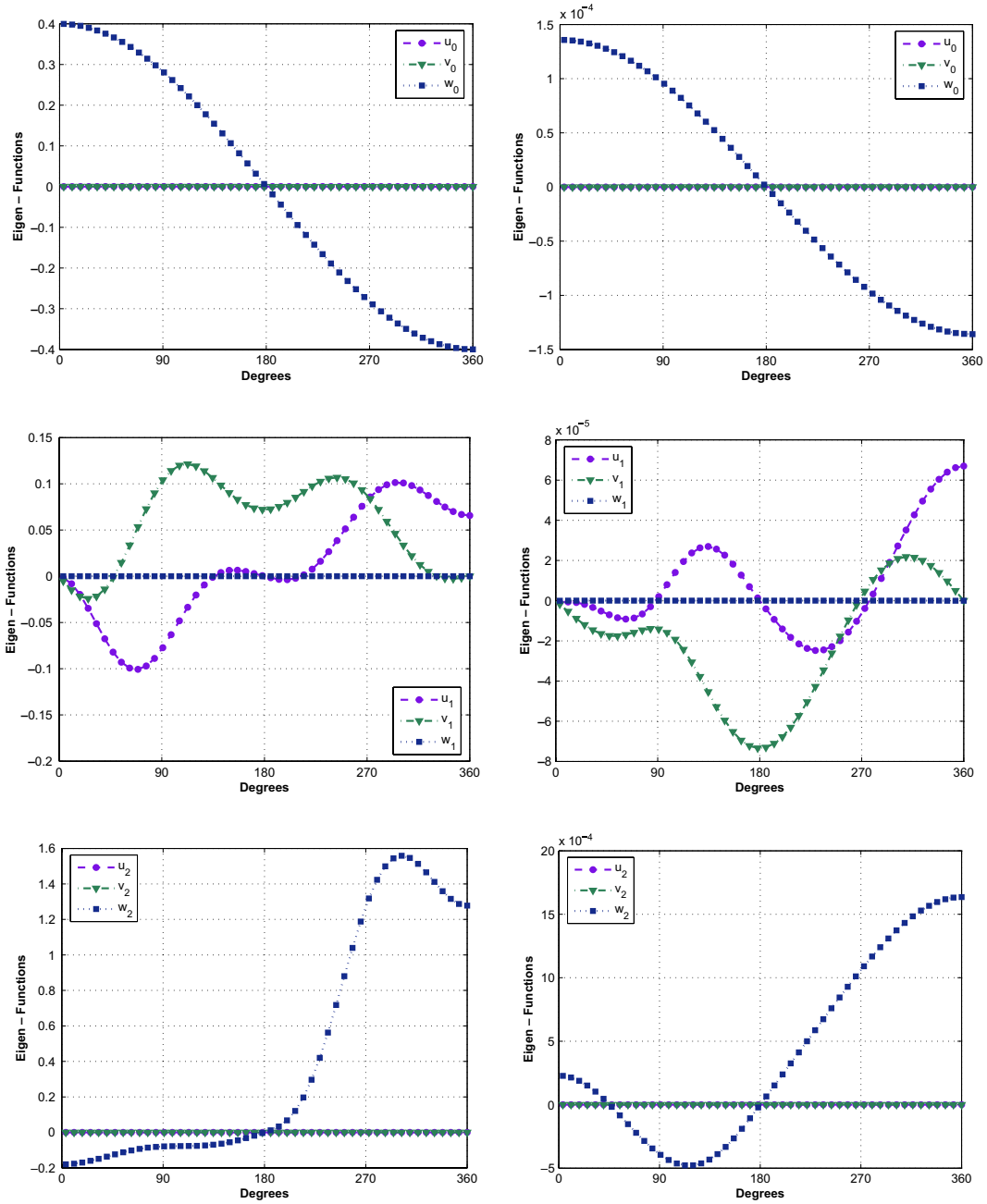

Fig. 16. Eigen-functions (left) and dual eigen-functions (right) associated with $\alpha_3 = 0.5$, computed by 8 elements, $p = 15$.

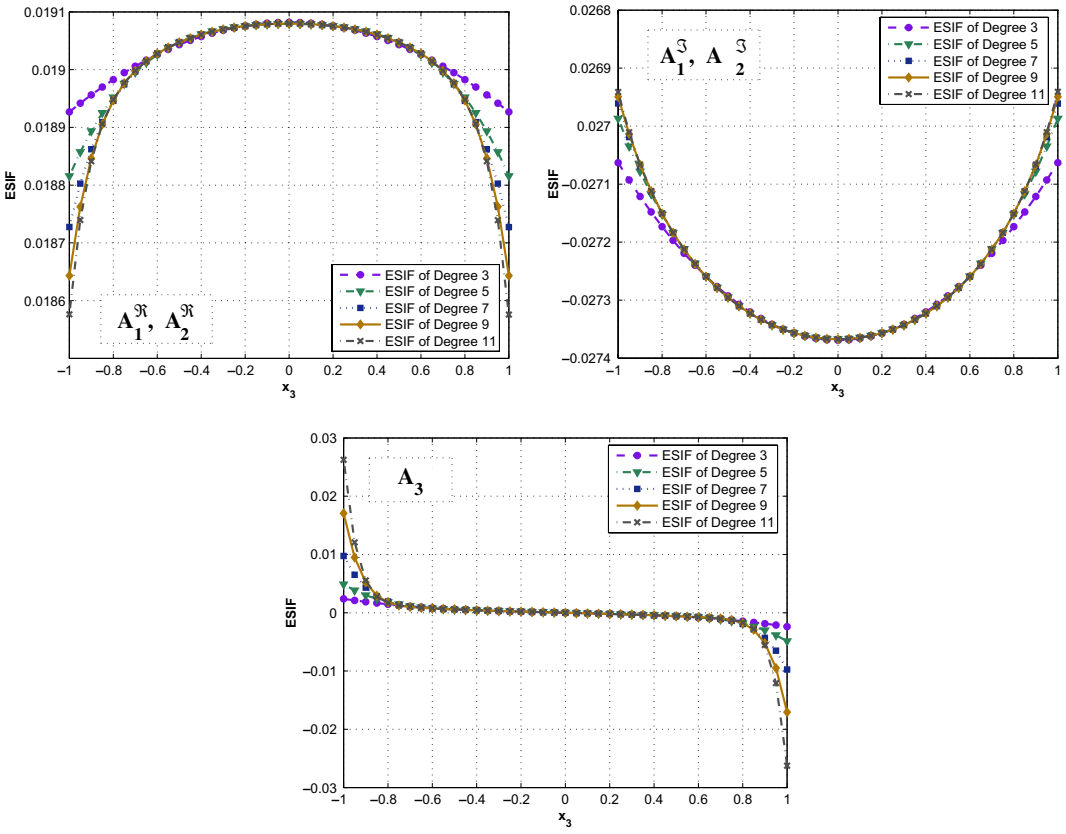

Fig. 17. ESIF extracted using $B^{(k)}$ with $k = 3, 5, 7, 9, 11$ for the CTS problem.

We present the relative error in percentage of the extracted $A^{\Re}_{1,2}(x_3), A^{\Im}_{1,2}(x_3), A_3(x_3)$ of order 3,4,5 in Fig. 11.

Notice that the relative error of the extracted ESIFs is less than 0.2%. These results indicate that the method is accurate and efficient, and may be applied to realistic engineering problems for which analytical solutions are unavailable as addressed in the next subsection.

6.2. Example B – CTS: crack at the interface of two anisotropic materials

Consider the classical compact tension specimen (CTS) of a constant thickness 2 $(-1 < x_3 < 1)$, shown in Fig. 12. The CTS's faces are traction free and it is loaded by bearing loads at the tearing holes having an equivalent force of 100 in the x_2 direction as seen in Fig. 13. Although the loading is independent of x_3, because of the vertex singularities at $x_3 = \pm 1$ we anticipate to see a variation in the ESIFs as the vertices are approached. The domain is discretized by using a p-FE mesh with geometrical progression towards the singular edge with a factor of 0.15 where the smallest layer in the vicinity of the edge is at $r = 0.15^2$. In x_3 direction we also used a mesh graded in a geometrical progression close to the vertex singularity at $x_3 = \pm 1$. Smallest layer in the vicinity of the vertex is $-1 < x_3 < -1 + 0.15^2, 1 < x_3 < 1 - 0.15^2$, see Fig. 13.

The CTS is made of two orthotropic materials as shown in Fig. 12. Both materials are made of the same high-modulus graphite-epoxy system (50) with different fiber orientation. The orientation of fibers of the upper material is along x_1 direction whereas the orientation at the lower material is along x_3 direction.

The first three eigen-values for this example problem, computed using a 8 elements model and $p = 15$ are given in (51). The eigen-functions, duals and shadows associated with the first three eigen-values are presented in Figs. 14–16 computed by 8 elements, $p = 15$.

We extract the ESIF A_1, A_2 and A_3 by increasing the polynomial order of approximation: 3, 5, 7, 9 and 11 at $R = 0.05$ (there was no noticeable difference between the ESIFs extracted at $R = 0.05$ and at $R = 0.1$). The extracted ESIFs are presented in Fig. 17.

One may notice the good convergence of the ESIFs as the order of the extraction polynomial is increased. Although the ESIFs are influenced by the vertex singularity at $x_3 = \pm 1$, as we increase their polynomial order the extracted ESIF converge closer to the vertices and provide a better approximation. This example demonstrate the efficiency and accuracy of the ESIF extraction method, and it's excellent results also in the close vicinity of the vertices.

7. Summary and conclusions

The series expansion representing the solution to elasticity problems in 3-D polyhedral multi-material anisotropic domains in the vicinity of an edge is addressed. The

weak-forms for the computation of eigen-functions complemented by shadow-functions and their associated edge stress intensity functions (ESIFs), which are functions along the edge, presented in [11] are refined and extended herein. In the case of anisotropic multi-material interfaces, analytic methods for the computation of eigen-pairs and shadows is impractical. Therefore the p-version of the finite element method is used for their computation. The numerical schemes are extended so to address complex eigen-functions and shadows and applied to multi-material anisotropic interfaces. The quasidual function method [4] is also extended for extracting complex ESIFs from finite element solutions.

We illustrate herein some pathological cases, among them the important crack configuration, for which the computation of the shadow-functions by numerical methods may fail. A heuristic remedy is proposed to alleviate the problem, shown to result in excellent approximations for the shadow-functions in several numerical examples. A rigorous mathematical analysis of these pathological cases is underway and will be reported in a future publications.

Two numerical examples for 3-D isotropic and anisotropic multi-material interfaces are provided for which the complex eigen-pairs and shadow functions are numerically computed and ESIFs extracted. The first example problem is tailored so to demonstrate the accuracy of the presented methods, and the functional representation of the complex ESIF. The second example problem is a typical problem in composite materials of a crack at the interface of two anisotropic materials. The complex ESIFs are computed, and the method shows excellent performance also close to the vertex singularities.

The application of p-FEMs for the computation of the dual shadow functions in conjunction with the quasi-dual functions method for the extraction of the edge stress intensity functions have been shown to provide a very accurate *functional representation* of ESIFs in any 3-D domain made of isotropic or anisotropic elastic material, provided the edges of interest are straight.

Acknowledgements

The authors thank Profs. Monique Dauge of the UMR-CNRS 6625-IRMAR, Universite de Rennes 1, Campus de Beaulieu, Rennes, France, for helpful discussions, remarks and support. This research was supported in part by the Israel Science Foundation (Grant No. 750/07).

Appendix A. The anisotropic material matrix in Cartesian and cylindrical coordinate systems

The material matrix $[E]$ (respectively $[\widetilde{E}]$) is a symmetric matrix

$$[E]=\begin{pmatrix} E_{11} & E_{12} & E_{13} & E_{14} & E_{15} & E_{16} \\ & E_{22} & E_{23} & E_{24} & E_{25} & E_{26} \\ & & E_{33} & E_{34} & E_{35} & E_{36} \\ & & & E_{44} & E_{45} & E_{46} \\ & & & & E_{55} & E_{56} \\ & & & & & E_{66} \end{pmatrix}, \tag{65}$$

where E_{ij} are the material properties expressed in a Cartesian system. The material matrix $[\widetilde{E}]$ is associated with $[E]$ via trigonometric relations:

$$\begin{aligned}
\widetilde{E}_{11} &= \frac{1}{8}(3E_{11}+2E_{12}+3E_{22}+4E_{66} \\
&\quad +4(E_{11}-E_{22})\cos(2\theta)+(E_{11}-2E_{12}+E_{22}-4E_{66}) \\
&\quad \times\cos(4\theta)E_{26})\sin(2\theta)+4(E_{16}-E_{26})\sin(4\theta), \\
\widetilde{E}_{12} &= \frac{1}{8}(E_{11}+6E_{12}+E_{22}-4E_{66} \\
&\quad -(E_{11}-2E_{12}+E_{22}-4E_{66})\cos(4\theta) \\
&\quad +4(-E_{16}+E_{26})\sin(4\theta)), \\
\widetilde{E}_{13} &= \frac{1}{2}(E_{13}+E_{23}+(E_{13}-E_{23})\cos(2\theta)+2E_{36}\sin(2\theta)), \\
\widetilde{E}_{14} &= \frac{1}{4}((3E_{14}+E_{24}-2E_{56})\cos(\theta)+(E_{14}-E_{24}+2E_{56}) \\
&\quad \times\cos(3\theta)-2(E_{15}+E_{25}-2E_{46}+(E_{15}-E_{25}-2E_{46}) \\
&\quad \times\cos(2\theta))\sin(\theta)), \\
\widetilde{E}_{15} &= \frac{1}{4}((3E_{15}+E_{25}+2E_{46}) \\
&\quad \times\cos(\theta)+(E_{15}-E_{25}-2E_{46}) \\
&\quad \times\cos(3\theta)+2(E_{14}+E_{24}+2E_{56}+(E_{14}-E_{24}+2E_{56}) \\
&\quad \times\cos(2\theta))\sin(\theta)), \\
\widetilde{E}_{16} &= \frac{1}{8}(4(E_{16}+E_{26})\cos(2\theta)+4(E_{16}-E_{26})\cos(4\theta) \\
&\quad -2(E_{11}-E_{22}+(E_{11}-2E_{12}+E_{22}-4E_{66})\cos(2\theta)) \\
&\quad \times\sin(2\theta)), \\
\widetilde{E}_{22} &= \frac{1}{8}(3E_{11}+2E_{12}+3E_{22}+4E_{66} \\
&\quad +4(-E_{11}+E_{22})\cos(2\theta)+(E_{11}-2E_{12}+E_{22}-4E_{66}) \\
&\quad \times\cos(4\theta)-8(E_{16}+E_{26})\sin(2\theta)+4(E_{16}-E_{26})\sin(4\theta)), \\
\widetilde{E}_{23} &= \frac{1}{2}(E_{13}+E_{23}+(-E_{13}+E_{23})\cos(2\theta)-2E_{36}\sin(2\theta)), \\
\widetilde{E}_{24} &= \frac{1}{4}((E_{14}+3E_{24}+2E_{56})\cos(\theta) \\
&\quad +(-E_{14}+E_{24}-2E_{56})\cos(3\theta)-(3E_{15}+E_{25}+2E_{46}) \\
&\quad \times\sin(\theta)+(E_{15}-E_{25}-2E_{46})\sin(3\theta)), \\
\widetilde{E}_{25} &= \frac{1}{4}((E_{15}+3E_{25}-2E_{46})\cos(\theta) \\
&\quad +(-E_{15}+E_{25}+2E_{46})\cos(3\theta)+(3E_{14}+E_{24}-2E_{56}) \\
&\quad \times\sin(\theta)+(-E_{14}+E_{24}-2E_{56})\sin(3\theta)), \\
\widetilde{E}_{26} &= \frac{1}{8}(4(E_{16}+E_{26})\cos(2\theta)+4(-E_{16}+E_{26})\cos(4\theta) \\
&\quad +2(-E_{11}+E_{22})\sin(2\theta) \\
&\quad +(E_{11}-2E_{12}+E_{22}-4E_{66})\sin(4\theta))
\end{aligned}$$

$$
\begin{aligned}
\widetilde{E}_{33} &= E_{33},\\
\widetilde{E}_{34} &= E_{34}\cos(\theta) - E_{35}\sin(\theta),\\
\widetilde{E}_{35} &= E_{35}\cos(\theta) + E_{34}\sin(\theta),\\
\widetilde{E}_{36} &= E_{36}\cos(2\theta) + (-E_{13} + E_{23})\cos(\theta)\sin(\theta),\\
\widetilde{E}_{44} &= \frac{1}{2}(E_{44} + E_{55} + (E_{44} - E_{55})\cos(2\theta) - 2E_{45}\sin(2\theta)),\\
\widetilde{E}_{45} &= E_{45}\cos(2\theta) + (E_{44} - E_{55})\cos(\theta)\sin(\theta),\\
\widetilde{E}_{46} &= \frac{1}{2}(2\cos(2\theta)(E_{46}\cos(\theta) - E_{56}\sin(\theta))\\
&\quad + ((-E_{14} + E_{24})\cos(\theta) + (E_{15} - E_{25})\sin(\theta))\sin(2\theta)),\\
\widetilde{E}_{55} &= E_{55}\cos(\theta)^2 + E_{44}\sin(\theta)^2 + E_{45}\sin(2\theta),\\
\widetilde{E}_{56} &= \sin(\theta)(E_{46}\cos(2\theta) + (-E_{14} + E_{24})\cos(\theta)\sin(\theta))\\
&\quad + \cos(\theta)(E_{56}\cos(2\theta) + (-E_{15} + E_{25})\cos(\theta)\sin(\theta)),\\
\widetilde{E}_{66} &= \frac{1}{8}(E_{11} - 2E_{12} + E_{22} + 4E_{66}\\
&\quad - (E_{11} - 2E_{12} + E_{22} - 4E_{66})\cos(4\theta)\\
&\quad + 4(-E_{16} + E_{26})\sin(4\theta)).
\end{aligned}
\tag{66}
$$

References

[1] T. Apel, V. Mehrmann, D. Watkins, Structured eigenvalue method for computation of corner singularities in 3D anisotropic elastic structures, Comput. Methods Appl. Mech. Engrg. 191 (2002) 4459–4473.

[2] L. Banks-Sills, P.A. Wawrzynek, B. Carter, A.R. Ingraffea, I. Hershkovitz, Methods for calculating stress intensity factors in anisotropic materials: Part II Arbitrary geometry, Engrg. Frac. Mech. 74 (8) (2007) 1293–1307.

[3] H. Blum, M. Dobrowolski, On finite element methods for elliptic equations on domains with corners, Computing 28 (1982) 53–63.

[4] M. Costabel, M. Dauge, Z. Yosibash, A quasidual function method for extracting edge stress intensity functions, SIAM J. Math. Anal. 35 (5) (2004) 1177–1202.

[5] M. Gosz, J. Dolbow, B. Moran, Domain integral formulation for stress intensity factor computation along curved three-dimensional interface cracks, Int. J. Solids Struct. 35 (15) (1998) 1763–1783.

[6] T. Ikeda, M. Nagai, K. Yamanaga, N. Miyazaki, Stress intensity factor analyses of interface cracks between dissimilar anisotropic materials using the finite element method, Engrg. Frac. Mech. 73 (2006) 2067–2079.

[7] R. Nahta, B. Moran, Domain integrals for axisymmetrical interface crack problems, Int. J. Solids Struct. 30 (15) (1993) 2027–2040.

[8] E. Pan, F.G. Yuan, Boundary element analysis of three-dimensional cracks in anisotropic solids, Int. J. Numer. Methods Engrg. 48 (48) (2000) 211–237.

[9] J.R. Rice, A path independent integral and the approximate analysis of strain concentration by notches and cracks, J. Appl. Mech. 35 (2) (1968) 379–386.

[10] Z. Yosibash, Computing edge singularities in elastic anisotropic three-dimensional domains, Int. J. Fracture 86 (3) (1997) 221–245.

[11] Z. Yosibash, N. Omer, Numerical methods for extracting edge stress intensity functions in anisotropic three-dimensional domains, Comput. Methods Appl. Mech. Engrg. 196 (2007) 3624–3649.

[12] Z. Yosibash, N. Omer, M. Costabel, M. Dauge, Edge stress intensity functions in polyhedral domains and their extraction by a quasidual function method, Int. J. Fracture 136 (2005) 37–73.

[13] Z.Q. Yue, H.T. Xiao, E. Pan, Stress intensity factors of square crack inclined to interface of transversely isotropic bi-material, Engrg. Anal. Boundary Elem. 31 (2007) 50–65.